

**Generic tool for numerical simulation of transformation-diffusion
processes in complex volume geometric shapes: application to
microbial decomposition of organic matter**

**Olivier MONGA^{a,b}, Frédéric HECHT^c, Serge MOTO^d, Bruno
MBE^d, Patricia GARNIER^e, Valérie POT^e**

^a IRD, UMMISCO, Unité de Modélisation Mathématique et Informatique des Systèmes Complexes, F-93143, Bondy, France

^b Cadi Ayyad University, Faculty of Sciences Semlalia, Department of Mathematics, BP 2390, Marrakech

^c Sorbonne Université, UMR 7618, Laboratoire Jacques Louis Lions, 75005 Paris

^d UMMISCO-Cameroun, UMI 209 UMMISCO, IRD, Sorbonne Université, university of Yaoundé

^e UMR 1402, ECOSYS, INRA, 78850, France

Corresponding author: Olivier Monga, Olivier.monga@ird.fr

Submitted to Computers and Geosciences

Abstract.

This paper presents a generic framework for the numerical simulation of transformation-diffusion processes in complex volume geometric shapes. This work follows a previous one devoted to the simulation of microbial degradation of organic matter in porous system at microscopic scale. We generalized and improved the MOSAIC method significantly and thus yielding a much more generic and efficient numerical simulation scheme. In particular,

regarding the simulation of diffusion processes from the graph, in this study we proposed a completely explicit and semi-implicit numerical scheme that can significantly reduce the computational complexity. We validated our method by comparing the results to the one provided by classical Lattice Boltzmann Method (LBM) within the context of microbial decomposition simulation. For the same datasets, we obtained similar results in a significantly shorter computing time (i.e., 10-15 minutes) than the prior work (several hours). Besides the classical LBM method takes around 3 weeks computing time.

1- Introduction

The up to date scientific challenges linked to ecology and environment monitoring motivate a growing interest regarding the numerical simulation of natural dynamics [Bultreys et al. 2015, Byrne et al. 2006, De Jong et al. 2004, Kolade et al. 2016, Sun et al. 2017, Uduak et al. 2013]. In parallel, the fast technological advances of image sensors makes possible to study biological and physical dynamics at microscopic scale and even nanoscale [Juyar et al. 2018, Kumi 2015, Gutteriez et al. 2018, Dong et al. 2009, Haslett 1995, Hilpert et al. 2001, Reeves et al. 1996]. The goal is a better understanding of microscopic processes in order to improve and to understand macroscopic models. Within the future, the purpose is to link microscopic data and models to macroscopic ones. Indeed, the use of real experiences in order to study the biological dynamics at fine micro-scale are very costly regarding: experimental equipment, engineering tasks, delivery times, data acquisition.... That is why, the way of computational modelling is nowadays strongly investigated. The aim of this paper is to propose a new generic numerical scheme much more efficient than the classical ones [Pot et al. 2015, Monga et al. 2014, Nguyen

et al. 2015]. Indeed, the two bottle necks of this task are : the geometrical data (spatial dimension) and the dynamics of the simulation (temporal dimension).

Dealing with the first bottle neck, we use previous works based on advanced geometrical modelling [Monga 2007, Monga et al. 2007, Ndeye et al. 2011]. The aim of these methods is to provide intrinsic and relevant piece wise approximation of pore space volume using basic geometrical primitives (balls, ellipsoids, cones, cylinders, generalized cylinders...). This geometrical modelling stage can be seen as data compression process (for instance 100M voxels can be represented by 1M balls).

The second bottle neck comes from the two different dynamics: the biological dynamics which is not uniform in space, the diffusion dynamics which is more classical but imposing a huge step time constraint in explicit Euler scheme. Our idea is to use non homogeneous time splitting and implicit Euler scheme for the diffusion part (no time step limitation and linear problem). We implemented a local adaptive explicit scheme to simulate biological dynamics. The implementation is described through details in section 3.

We have validated the whole scheme within the frame of scenarios regarding the microbial decomposition of dissolved organic matter in soil. The results are in accordance with the ones of classical voxel-based simulation algorithms such as Lattice Boltzmann Method (LBM) [Pot et al. 2015, Schaap et al. 2007, Shan et al. 1993, Shan et al. 2014, Sukop et al. 2008] or Partial Differential Equations (PDE) [Nguyen et al. 2015, Resat et al. 2012, Falconer et al. 2008]. For instance, we got good fitting with the LBM flow charts provided by the method described in [Pot et al. 2015]. The classical LBM scheme can yield to heavy computing time (up to several weeks). The previous graph based approach described in [Monga et al. 2014] is faster but is

roughly inversely proportional to the diffusion coefficients (up to 15 hours with a high diffusion coefficient using a common PC). Finally, the cost of the algorithm presented here does not depend on the diffusion coefficient values (less than half hour on same data set). Indeed, the most spectacular computing time gain is due to the use of an implicit scheme to simulate diffusion processes from the graph of the primitives, which breaks the time step limit of the explicit scheme. In this specific case, the implicit scheme leads to solve a huge and sparse linear system well-conditioned that can be done very efficiently thanks to dozen of iterations of conjugated gradient.

Besides, in a methodological point of view, the formalization of our method allows implementing numerical simulation of various dynamics only by changing the values of certain parameters. We come up with a general tool which can be used easily within many applicative contexts. In the present paper, we focus on the simulation of microbial decomposition of organic matter at microscopic scale from Computed Tomography (CT) images. We validated our method using the same data set than the one described in [Mbe et al. 2021]. Indeed, this paper describes the mathematical and algorithmic schemes used in [Mbe et al. 2021]. This can open new horizons for numerical simulation of biological dynamics in soil.

The rest of the paper is organized as follows: Section 2 deals with pore space geometrical modelling, which is a prerequisite in order to implement graph based simulation schemes. Section 3 presents the semi-implicit numerical scheme. Finally, Section 4 validates our approach, and presents comparative evaluations with respect to classical LBM.

2- Pore network geometrical modelling

We represent pore space using a set of geometrical primitives disjoint, tangent or intersecting weakly two by two. These primitives are computed from micro-scale computed tomography image and form a piece wise approximation of the pore space at microscopic scale [Monga et al. 2007, Kengue et al. 2019, Ngom et al. 2012, Ngom et al. 2011, Monga 2007]. From this set of primitives, we compute an attributed adjacency valuated graph relying upon the true representation of the pore space. In this graph, each node is attached to a primitive assimilated to the intuitive notion of pore, and each arc to an adjacency between two primitives. The union of all primitives approximates the pore space. In this paper, we validate our algorithms from real image dataset. As described in [Monga et al. 2007], we use the minimum set of balls recovering the skeleton of the shape. It provides a precise, relevant and compact representation of the pore space much more tractable for numerical simulation than the primary set of voxels, and more realistic than idealized pore networks models [Bultrey 2015]. In the present work, we use balls as basic primitives. We could also have implemented the same numerical simulation scheme by using others primitives like ellipsoids [Kengue et al. 2019]. The advantage of ellipsoids based pore space representation would have been a better compacity of the representation (ratio of about 1/10 for the graph size). The drawback would have been the higher computational cost of the geometrical stage.

3- Theoretical framework for numerical simulation

4.1- Problem statement

Let $G_t(N, E)$ be the non-oriented attributed relational graph of the geometrical primitives describing pore space at time t , where $N = \{N_1, N_2, \dots, N_q\}$ is the set of nodes and $E = \{(N_{i_1}, N_{j_1}), (N_{i_2}, N_{j_2}), \dots (N_{i_r}, N_{j_r})\}$ is the set of arcs.

At each node N_i , we attach the vector $F^i = (f_1^i, f_2^i, \dots, f_k^i, \dots, f_p^i)$ defining the feature vector of node N_i .

The components of F^i include the descriptors of the associated geometrical primitive $(f_1^i, f_2^i, \dots, f_k^i)$ and the “biological” parameters of the primitive $(f_{k+1}^i, f_{k+2}^i, \dots, f_p^i)$. We notice that for the scenarios reported in this paper, we will consider that the pore space shape does not vary over time. It means that the part of F^i attached to the geometrical features does not depend on time. Besides, the biological features attached to each pore will vary overtime. Therefore, the part of F^i attached to the biological features depends on time. However, our methodological framework allows easily to take into account pore space geometry changes over time. In forthcoming works, we will consider that the pore space geometry will vary also over time.

Coming back to the equations, if the geometrical primitive is a ball then $(f_1^i, f_2^i, f_3^i, f_4^i)$ corresponds to the coordinates of the center and f_4^i to the radius [Monga et al. 2014, Monga et al. 2009]. If the geometrical primitive is an ellipsoid, the set $(f_1^i, f_2^i, f_3^i, f_4^i, f_5^i, f_6^i \dots)$ corresponds to the coordinates of its center, its three radiuses and the direction of the principal axis [Kemgue, Monga et al. 2019]. The biological parameters correspond to the mass of microorganisms, organic matters, enzymes, etc contained within the geometrical primitive. The geometrical primitives attached to each node are assumed to be disjunct, tangent or intersecting weakly two by two, and thus forming a piecewise approximation of the pore space [Monga et al. 2019, Monga et al. 2009, Ndeye, Monga et al. 2012, Monga 2007].

Let E be the set of arcs of graph G_t . Each arc $E_{ij} = (N_i, N_j)$ of the graph is attached to two adjacent geometrical primitives N_i and N_j . At each arc E_{ij} , we attach the characteristics of the

adjacency of the two geometrical primitives N_i and N_j : area of the contact surface, distance between the two inertia centers. The neighborhood $\mathcal{V}(N_i)$ of a node N_i is the set of nodes connected to N_i by an arc can be defined as follows:

$$\mathcal{V}(N_i) = \{N_j \in N \setminus (N_i, N_j) \in E\} \quad (1)$$

We assume that the biological dynamics correspond to the transformation of the “biological” parameters attached to each node: $(f_{k+1}^i, f_{k+2}^i, \dots, f_p^i)$. These transformations are defined from the biological dynamics model: organic matter assimilation, biomass degradation, breathing, enzymes emission, etc. Indeed, the biological parameters match with masses of various matters contained within the node geometrical volume primitive: solid organic matter, dissolved organic matter, microorganisms, enzymes, carbon dioxide. In vector, $(f_{k+1}^i, f_{k+2}^i, \dots, f_p^i)$ we assume that the masses are expressed using the same mass unit ($\mu g, g \dots$). Transformation equations are expressed as a function of $T((x_1, x_2, \dots, x_p), \delta t)$ as follows:

$$T: \mathbb{R}^p \times \mathbb{R} \rightarrow \mathbb{R}^p / T((x_1, x_2, \dots, x_p), \delta t) = (y_1, y_2, \dots, y_p) \quad (2)$$

where (x_1, x_2, \dots, x_p) are the values of the biological parameters at a time t and (y_1, y_2, \dots, y_p) the values at time $(t + \delta t)$.

Given that the total mass is conserved, we have:

$$x_1 + x_2 + \dots + x_p = y_1 + y_2 + \dots + y_p \quad (3)$$

For instance, in the case of the biological dynamics model described in (Monga et al 2014) the set of biological parameters at a given node N_i is $(x_1, x_2, x_3, x_4, x_5)$ where: x_1 is the microbial biomass (MB), x_2 is the mass of dissolved organic matter (DOM), x_3 is the mass of soil organic matter (SOM), x_4 is the mass of fresh organic matter (FOM), x_5 is the mass of carbon dioxide (CO₂). If v is the volume of the primitive attached to the node ($v = f_m^i$) then $\frac{x_2}{v} = c_{DOM}$ is the concentration of DOM within the primitive attached the node. The DOM comes from the decomposition of the SOM (slow decomposition) and of the FOM (fast decomposition). The microorganisms grow by assimilating DOM, breath by producing carbon dioxide. Afterward, they are transformed into SOM and DOM when they die.

When applying the biological model described in [Monga et al. 2014] we get:

$$\left\{ \begin{array}{l} y_1 = x_1 - \rho x_1 \delta t - \mu x_1 \delta t + \frac{v_{DOM} c_{DOM}}{\kappa_b + c_{DOM}} x_1 \delta t = x_1 + \delta b_i^1 \\ y_2 = x_2 + \rho_m \mu x_1 \delta t - \frac{v_{DOM} c_{DOM}}{\kappa_b + c_{DOM}} x_1 \delta t + v_{SOM} x_3 \delta t + v_{FOM} x_4 \delta t = x_2 + \delta b_i^2 \\ y_3 = x_3 + (1 - \rho_m) \mu x_1 \delta t - v_{SOM} x_3 \delta t = x_3 + \delta b_i^3 \\ y_4 = x_4 - v_{FOM} x_4 \delta t = x_4 + \delta b_i^4 \\ y_5 = x_5 + \rho x_1 \delta t = x_5 + \delta b_i^5 \end{array} \right. \quad (4)$$

where ρ is the relative respiration rate, μ the relative mortality rate, ρ_m the proportion of MB returning to DOM (the other fraction returns to SOM), v_{FOM} and v_{SOM} the relative decomposition rate of FOM and SOM, v_{DOM} and κ_b the maximum relative growth rate of MB and constant of half saturation of DOM.

We notice that Equation (4) can be summarized as follows.

For each node of the graph:

$$Y = C(X, \delta t) \text{ where } Y=(y_1, y_2, y_3, y_4, y_5) \text{ and } X=(x_1, x_2, x_3, x_4, x_5)$$

For the whole graph :

$$B^{N+1} = B^N + OP(B^N, \delta t) \Leftrightarrow \delta B = OP(B, \delta t)$$

where B^N and B^{N+1} are respectively the biological features of the graph at time t and $t+\delta t$

Due to mass conservation, for each node N_i we have:

$$\delta b_i^1 + \delta b_i^2 + \delta b_i^3 + \delta b_i^4 + \delta b_i^5 = 0 \quad (5)$$

which implies also global mass conservation for the whole graph:

$$\sum_{i=1}^{i=q} \sum_{j=1}^{j=5} \delta b_i^j = 0 \quad (6)$$

Practically, biological transformation defined by function T happens jointly with diffusion processes in the sense of Fick Laws [Fick 1855]. For numerical simulation of the whole process, we can implement transformation and diffusion processes in parallel or sequentially.

Let us suppose that we have a diffusion process of DOM (dissolved organic matter) in water with a diffusion coefficient C_{dom} .

Let us attach to each node N_i of the graph $G_t(N,E)$ the following features:

$m_i(t) = x_2$: mass of DOM at time t for node N_i

G_i : center of inertia of the region attached to the node (center of the ball)

v_i : volume of the region

To each arc $E_{i,j} = (N_i, N_j)$ is attached:

$d_{i,j}$: Euclidean distance between the two centers of inertia of nodes i and j

$s_{i,j}$: Area of contact surface between the two regions attached to nodes. In the case of the optimal ball network (Monga et al. 2007) we set the area of contact to the disk whose radius is the harmonic mean of the radiuses of the two adjacent balls ($\frac{1}{r} = \frac{1}{r_1} + \frac{1}{r_2}$).

The DOM concentration c_i in N_i at time t is : $c_i(t) = \frac{m_i}{v_i}$

We note $\delta_{c_{ij}}$ the difference of concentration between two nodes N_i and N_j linked by an arc $E_{i,j}$:

$$\delta_{c_{ij}} = c_i - c_j \quad (7)$$

We note that : $d_{i,j} = d_{j,i} > 0$; $s_{i,j} = s_{j,i} > 0$; $\delta_{c_{ij}} = -\delta_{c_{ji}}$ (it can be negative)

According to first Fick law, the flow between a node N_i to a node N_j of the graph for a time step δt is :

$$F_{i,j} = \frac{-D_c s_{i,j} \delta_{c_{ij}}}{a_{i,j}} \delta t \quad (8)$$

where D_c is the DOM diffusion coefficient in water.

Let $\mathcal{V}(N_i)$ be the set of adjacent nodes N_j of the node N_i . The total variation of DOM mass at node N_i is,

$$\delta m_i = \sum_{N_j \in \mathcal{V}(N_i)} (-D_c s_{ij} \frac{\delta_{c_{ij}}}{a_{ij}} \delta t) \quad (9)$$

thus, for the DOM diffusion process between time t and time $t + \delta t$ we get,

$$y_2 = x_2 + \delta m_i = x_2 + \sum_{N_j \in \vartheta(N_i)} (-D_c s_{ij} \frac{\delta c_{ij}}{d_{ij}} \delta t) \quad (\mathbf{10})$$

By construction, we have mass conservation in the whole graph, i.e.,

$$\sum_{i=1}^{i=q} \delta m_i = 0 \quad (\mathbf{11})$$

The diffusion simulation between t and $t + \delta t$ can be reduced to applying synchronously Eq. (10) to each node N_i . Then, from graph at time t (G_t) we compute the graph at time $t + \delta t$ ($G_{t+\delta t}$).

4.2- Explicit numerical scheme

Let us suppose that we want to simulate the dynamics between time t and $t + \Delta t$.

This is equivalent of computing a graph at time $t + \Delta t$ from the graph at time t . Let G_t be the graph at time t and $G_{t+\Delta t}$ be the graph at time $t + \Delta t$. We compute $G_{t+\Delta t}$ from G_t thanks to an iterative process which consists in calculating: $G_{t+\delta t}, G_{t+2\delta t}, \dots, G_{t+\Delta t}$ where $\delta t = \frac{\Delta t}{n}$. There is two ways of implementing the explicit scheme. Either the transformation and diffusion processes are simulated in a synchronous (parallel) way or in an asynchronous (sequential) manner.

4.3- Explicit synchronous scheme: transformation, diffusion

At the first iteration we compute $G_{t+\delta t}$ from G_t by means of equations (4) and (10). For each node N_i of graph G_t , we compute the biological parameters at time $t + \delta t$ from the ones at time t using the following method. Let $(x_1, x_2, x_3, x_4, x_5)$ be the biological parameters at time t and $(y_1, y_2, y_3, y_4, y_5)$ be the biological parameters at time $t + \delta t$. From equations (4) and (10) one can express,

$$\left\{ \begin{array}{l} y_1 = x_1 + \delta b_i^1 \\ y_2 = x_2 + \delta b_i^2 + \delta m_i \text{ (12)} \\ y_3 = x_3 + \delta b_i^3 \\ y_4 = x_4 + \delta b_i^4 \\ y_5 = x_5 + \delta b_i^5 \end{array} \right.$$

Same as for equation (4) we can summarize equation (12) as follows:

$B^{N+1} = B^N + \delta B$ where B^N and B^{N+1} are respectively the biological parameters of the nodes of the graph at time t and $t+\delta$

The application of Eq. (12) to each node of G_t allows computing $G_{t+\delta t}$. However, the numerical scheme is coherent only if, $y_1, y_2, y_3, y_4, y_5 \geq 0$ because a mass cannot be negative. We use the same principle to compute $G_{t+(n+1)\delta t}$ from $G_{t+n\delta t}$.

Practically, if the time step δt is too big regarding the speediness of the dynamics then we may get negative values for some y_i . In this case, the time step δt must be reduced in order at least providing values of y_1 nearly positive. In practice, if some values of y_i are weakly negative for some nodes N_i , we round them to 0 by taking the needed mass in other nodes by conserving the ratio between the concentrations. Later, we will describe precisely the backtracking technique, which has been implemented to avoid this issue.

4.4- Explicit asynchronous scheme: transformation and diffusion

In this case, we will process sequentially the diffusion process and the transformation process. The application of Eq. (4) to each node of G_t allows simulating the transformation process. We get an updated graph $G_{t+\delta t}^1$. Afterwards, we apply Eq. (10) to each node of $G_{t+\delta t}^1$ in order to simulate diffusion process. We get an updated graph $G_{t+\delta t}^2$ corresponding to graph $G_{t+\delta t}^1$. We use the same principle to compute $G_{t+(n+1)\delta t}$ from $G_{t+n\delta t}$

4.5- Negative values processing method

Practically, in order to save computing time, we do not impose a strict positivity of the y_i , both for synchronous and asynchronous explicit scheme. Indeed, we define a maximum percentage of the negative values versus the total mass. We set to zero the negative values and took the required mass in other nodes.

Let $G_{t+\delta t}$ be the updated graph. We note $(y_1^i, y_2^i, \dots, y_5^i)$ the “mass vector” (biological parameters) attached to node N_i . The total mass of y_j^i in the whole graph at time $t + \delta t$ is,

$$M_j^{t+\delta t} = \sum_{i=1}^{i=q} y_j^i \quad (13)$$

Let us define $H_{t+\delta t}^j$ as the “negativity” of the component j of the mass vectors of graph $G_{t+\delta t}$ as follows:

$$H_{t+\delta t}^j = -\sum_{i=1}^{i=q} \min(0, y_j^i) \quad (14)$$

If for some j we have $H_{t+\delta t}^j \geq p_{neg} M_j^{t+\delta t}$ then the result is considered as non-valid and we backtrack using a smaller step time. Practically, we set p_{neg} to a value the range of, $\left[\frac{1}{100}, \frac{5}{100}\right]$.

If for each j we have $H_{t+\delta t}^j < p_{neg} M_j^{t+\delta t}$ then we set to 0 the negative y_j^i by taking masses in other nodes proportionally to the concentration. If $H_{t+\delta t}^j > 0$, then we consider all strictly positive y_j^i . Let us note $c_j^i = \frac{y_j^i}{v_i}$ be the concentration of matter j in node i . We set y_j^i to $y_j^i - \frac{c_j^i}{\sum_{i=1}^{i=q} c_j^i} H_{t+\delta t}^j$. We also set all strictly negative y_j^i to 0. This method allows getting positive values for the masses by preserving mass conservation. Of course, it can be used only if the “negativity” of the masses is low.

4.6- Backtracking time step scheme

For both synchronous and asynchronous explicit scheme, we implement a backtracking strategy for dealing with the situations when for some j we have $H_{t+\delta t}^j \geq p_{neg} M_j$. This means that the time step was too big regarding the dynamic.

Using the numerical scheme described previously we compute iteratively $G_t, G_{t+\delta t}, G_{t+2\delta t}, G_{t+3\delta t} \dots G_{t+n\delta t} \dots G_{t+\Delta t}$. If for $G_{t+k\delta t}$ we have,

$$\exists j / H_{t+k\delta t}^j \geq p_{neg} M_j^{t+k\delta t}$$

This means that the time step δt to calculate $G_{t+k\delta t}$ from $G_{t+(k-1)\delta t}$ was too high regarding the dynamics. In this case we use $\frac{\delta t}{2}$ instead of δt and then we calculate $G_{t+(k-1)\delta t+\frac{\delta t}{2}}$. Afterward, we continue the simulation with $\frac{\delta t}{2}$ instead of δt and iterate the same back tracking process.

This back tracking process allows coping with the cases where the initial value of δt is too high. Practically we start with an intermediate value of δt according to previous simulations. Of course, the most practical way would be to use a very small time step at the beginning but the computing time could be very high.

4.7 Computing time issues

We have implemented the three numerical schemes described above.

When the diffusion coefficient is high, the numerical simulation of diffusion processes by means of explicit schemes yields a high computational complexity, i.e., up to one day of computing time with a standard PC. Moreover, in most cases, the diffusion process is slower than the transformation process.

Therefore, we use one step time for the diffusion process and one step time for the transformation process.

Practically, we use mostly the asynchronous diffusion-transformation explicit scheme where the step time for the diffusion process is δt and the one for the transformation process is Δt . In fact, we simulate first the diffusion process between t and $t + \Delta t$ using Eq. (10) and step time δt . In this way we can get the updated graph after diffusion and then we apply to the graph the Eq. (4) in order to simulate transformation processes. This is the reason why we have also

implemented a numerical implicit scheme to simulate diffusion process, which poses a far greater computational cost.

4.8- Implicit scheme for simulation of diffusion process

Numerical implicit scheme for diffusion process simulation saves significant computing time. This is also the first attempt used for simulating diffusion processes from an adjacency relational graph of geometrical primitives. Below we detail the main principles of the proposed implicit scheme.

Let $G_t(N,E)$ be the non-oriented graph of the geometrical primitives describing pore space at time t as defined previously. N is the set of nodes of G and E the set of arcs. At each node N_i is attached a geometrical primitive (a ball) and the mass of carbon (DOC) contained in the ball at time t .

Thus, we attach to each node the following features:

- $m_i(t)$: mass of DOM at time t :
- G_i : center of inertia of the region attached to the node (center of the ball);
- v_i : volume of the region

To each arc $E_{i,j} = (N_i,N_j)$ is attached:

- $d_{i,j}$: Euclidean distance between the two centers of inertia of nodes i and j
- $s_{i,j}$: area of contact surface between the two regions attached to nodes

The carbon concentration c_i in N_i is : $c_i = \frac{m_i}{v_i}$

We note $\Delta_{c_{ij}}$ as the difference of concentration between two nodes N_i and N_j linked by an arc $E_{i,j}$. It can be expressed as follows:

$$\Delta_{c_{ij}} = c_i - c_j \quad (15)$$

We note that : $d_{i,j} = d_{j,i} > 0$; $s_{i,j} = s_{j,i} > 0$; $\Delta_{c_{ij}} = -\Delta_{c_{ji}}$ (it can be negative)

According to the first Fick law the flow between a node N_i to a node N_j of the graph for a time step dt is,

$$F_{i,j} = \frac{-D_c s_{i,j} \Delta_{c_{ij}}}{d_{i,j}} dt \quad (16)$$

where D_c is the diffusion coefficient of DOM in water.

Let p be the number of node in the graph of the connected component considered.

Let $\vartheta(N_i)$ be the set of adjacent nodes N_j of the node N_i . The total variation of carbon mass at node N_i can be expressed as,

$$\frac{\partial m_i}{\partial t} = \sum_{N_j \in \vartheta(N_i)} -D_c s_{ij} \frac{\Delta c_{ij}}{d_{ij}} \quad (17)$$

$$m_i(t + dt) = m_i(t) + dm_i \quad (18)$$

The following equation is valid,

$$\frac{\partial m_i}{\partial t} = v_i \frac{\partial c_i}{\partial t} \quad (19)$$

since $m_i = v_i c_i$ and v_i does not vary depending on the time

We use an iterative computation of the diffusion. The time between two iterations k and $k+1$ is dt . We consider that the difference of concentration between two iterations k and $k+1$ is expressed as follows:

$$\left(\frac{\partial c_i}{\partial t}\right)^{(k+1)} = c_i^{k+1} - c_i^k \quad (19)$$

We note :

$$\theta_{ij} = D_c \frac{s_{ij}}{d_{ij}} dt \quad (20)$$

Thus by combining equations (17) and (19) and setting dt to 1 it yields,

$$\left(\frac{\partial c_i}{\partial t}\right)^{(k+1)} = \sum_{N_j \in \vartheta(N_i)} -\theta_{ij} \frac{c_i^{k+1} - c_j^{k+1}}{v_i} \quad (21)$$

Combining Eq.s (19) and (21) yields,

$$c_i^k = \left(1 + \frac{1}{v_i} \sum_{N_j \in \vartheta(N_i)} \theta_{ij}\right) c_i^{k+1} - \frac{1}{v_i} \sum_{N_j \in \vartheta(N_i)} \theta_{ij} c_j^{k+1} \quad (22)$$

From Eq. (22) we can further express as follows:

$$\begin{bmatrix} c_1 \\ c_2 \\ \vdots \\ c_p \end{bmatrix}^k = \begin{pmatrix} \frac{1}{v_1} & \cdots & 0 \\ \vdots & \ddots & \vdots \\ 0 & \cdots & \frac{1}{v_p} \end{pmatrix} \begin{pmatrix} v_1 + \sum_{N_j \in \vartheta(N_1)} \theta_{1,j} & \cdots & -\theta_{1,p} \\ \vdots & \ddots & \vdots \\ -\theta_{p,1} & \cdots & v_p + \sum_{N_j \in \vartheta(N_p)} \theta_{p,j} \end{pmatrix} \begin{bmatrix} c_1 \\ c_2 \\ \vdots \\ c_p \end{bmatrix}^{k+1} \quad (23)$$

Moreover,

$$b = \begin{bmatrix} c_1 \\ c_2 \\ \vdots \\ c_p \end{bmatrix}^k, u = \begin{bmatrix} c_1 \\ c_2 \\ \vdots \\ c_p \end{bmatrix}^{k+1}$$

$$A = \begin{pmatrix} v_1 + \sum_{N_j \in \vartheta(N_1)} \theta_{1,j} & \cdots & -\theta_{1,p} \\ \vdots & \ddots & \vdots \\ -\theta_{p,1} & \cdots & v_p + \sum_{N_j \in \vartheta(N_p)} \theta_{p,j} \end{pmatrix}, V = \begin{pmatrix} \frac{1}{v_1} & \cdots & 0 \\ \vdots & \ddots & \vdots \\ 0 & \cdots & \frac{1}{v_p} \end{pmatrix} \quad (24)$$

We note that $\theta_{i,j} = \theta_{j,i}$ and $\theta_{ij} = 0$ when $j \notin \vartheta(N_i)$ then the matrix A is symmetrical and very sparse. Eq. (24) yields,

$$V A u = b \Rightarrow A u = V^{-1}b \quad (25)$$

The vector $V^{-1}b = c$ contains the mass attached to the node at iteration k . The vector u contains the concentrations attached to the nodes at iteration $(k+1)$. We solve Eq. (25) thanks to preconditioned conjugate gradient (PCG) method with diagonal preconditioner (Jacobi's preconditioner).

At each iteration, the discrete unknown vector u is computed by the solution of the linear system $A u = c$. As the system matrix A is symmetric, positive definite and very large, we chose to use the conjugated gradient method [ref] to solve this system, which will be detailed next.

4.9- Principle and algorithm of the conditioned conjugated gradient

The conjugated gradient enables solving a linear system $A u = c$, where A is a symmetric and positive definite matrix of size $n \times n$. It is based on the minimization of the following quadratic function $E: \mathbb{R}^n \rightarrow \mathbb{R}$; $E(x) = \frac{1}{2}(Ax, x) - (c, x)$

We can find a detailed description in [Quartenori et al. et al. 2007]. As the matrix M does not have a good condition number, we chose to use the conditioned conjugated gradient, in order to accelerate the convergence. For memory, if a matrix does not have a good condition number, the conjugated gradient method is very sensitive to rounded errors. So using an iterative method will not be possible, as the convergence will be difficult. The principle consists of multiplying the system by a matrix that is simple to invert, in order that the obtained matrix has a better condition number. We can find a full description and examples of condition matrices in [Quarteroni et al. 2007].

4.10- Computing time issues

Practically, we got exactly the same final simulation results using the explicit or implicit numerical schemes described above. The use of the asynchronous numerical scheme (implicit scheme for simulation – explicit scheme for biological transformations) allows to reduce the

computing time with a ratio at least 10 that is considerable. Indeed, when starting to use implicit schemes for diffusion simulation, we never get back to explicit schemes.

5-Model validation by comparison with Lattice Boltzmann Method (LBM)

5.1 Validation scheme

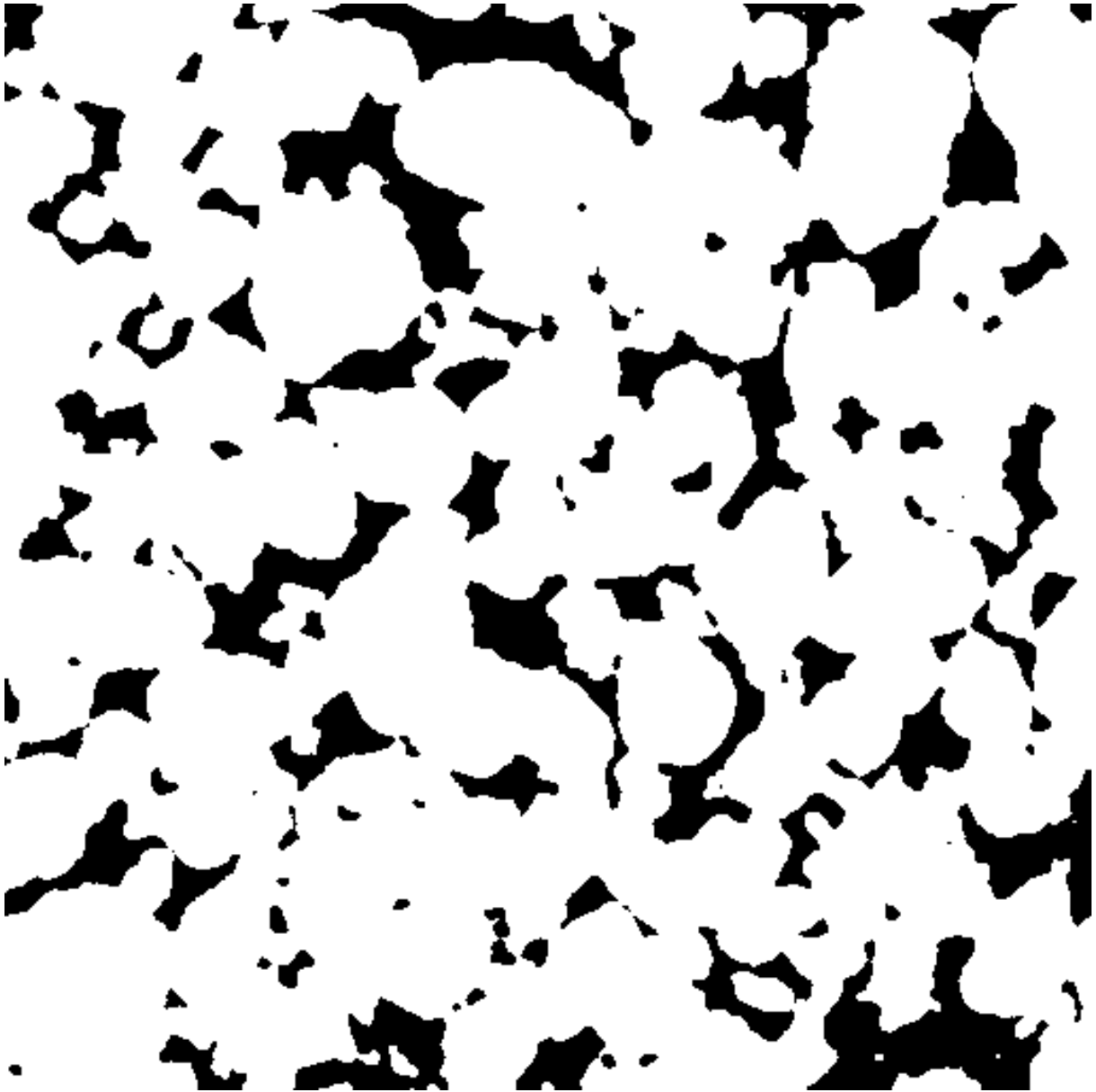
We have implemented and tested all the numerical schemes described above for the data set used in [Mbe et al. 2021]. If the step time is enough small the simulation output is the same but the computing time varies with a ratio up to 20. By far, the most efficient computational scheme is the one using the implicit numerical scheme to simulate diffusion processes. We have compared the simulation results provided by our method with the ones of Lattice Boltzmann Method (LBM) [Genty and Pot 2014, Mbe et al. 2021]. We obtained results in good agreement with a computing time around 15'-30' CPU instead of around 200h CPU for classical LBM (on a regular PC). The reasons are twofold. First, the optimal ball network provides a much more compact geometrical pore space representation than the rough voxel-based representation [Monga et al. 2007]. Indeed, we could also have used the ellipsoid based representation to get an even more compact geometrical representation [Kemgwe et al. 2019]. Second, the implicit numerical scheme, applied to the ball network to simulate diffusion, is much more efficient than voxel-based classical schemes. The previous statement, regarding the much lower computational cost of primitive-based methods versus voxel-based methods, applies not only for LBM but for any numerical scheme based on voxels as for instance Partial Differential Equations schemes [Nguyen et al. 2015, Nguyen et al. 2013] .

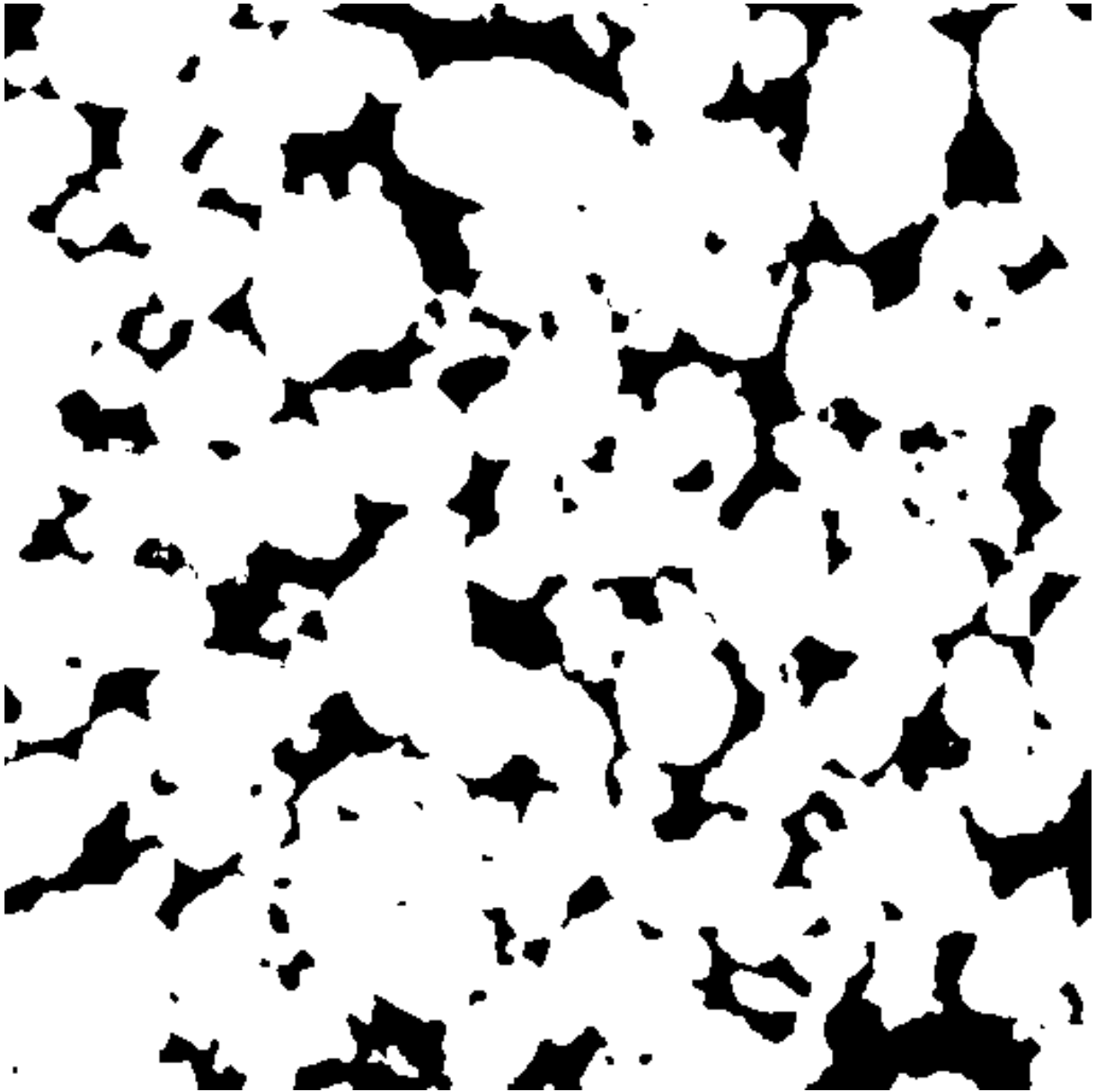
5.2 Pore space voxel based representation

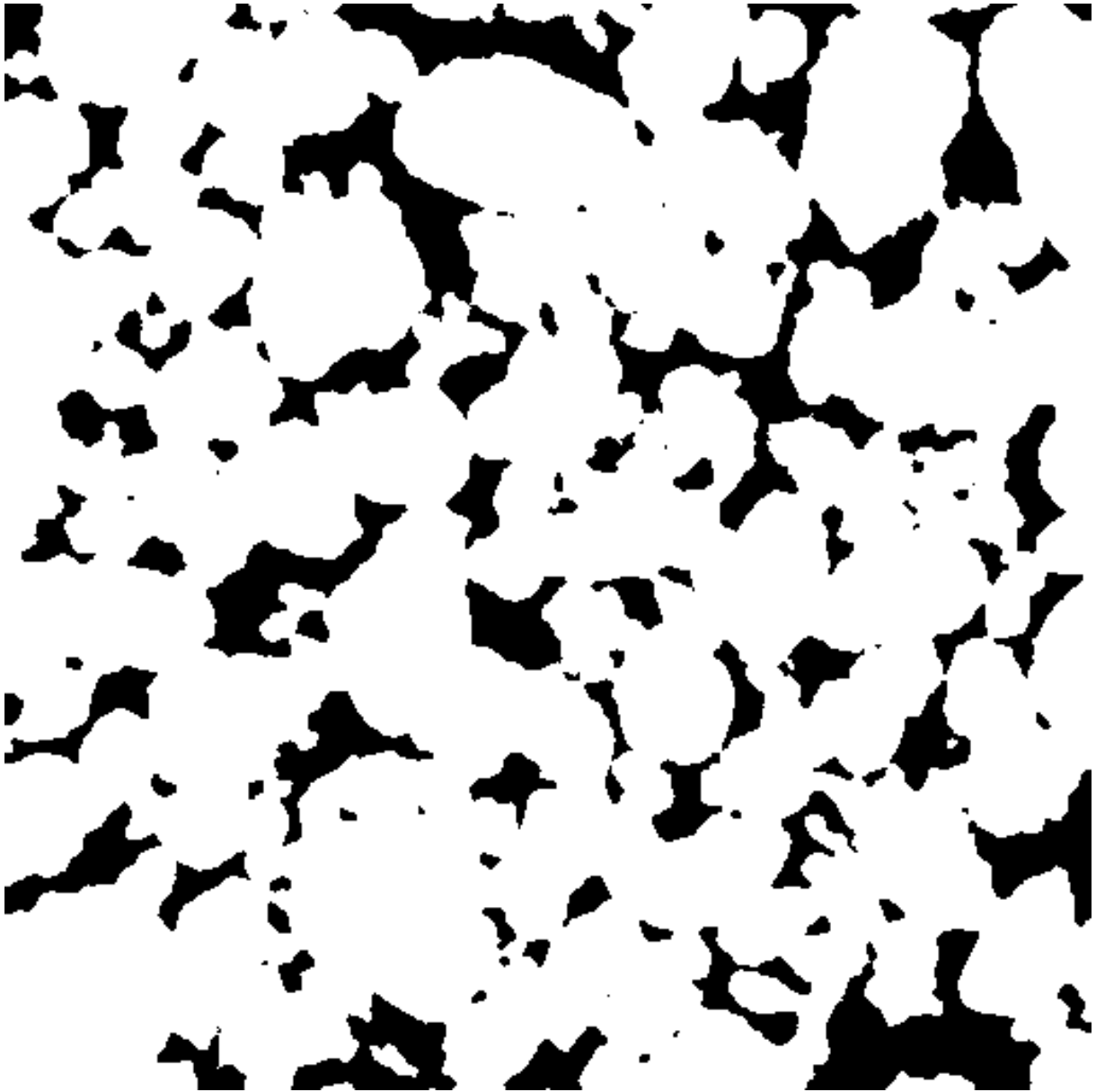
The initial pore space representation consists in 3D binary image of sizes 512x512x512 (see figure 1) where the pore space voxels are labeled (black color in the figure). This initial voxel based description of pore space comes from 3D grey level Computed Tomography (CT) image of soil sample. The homogeneous spatial resolution of the image is: 24 μ m x 24 μ m x 24 μ m.

The data image is the same as the one described in [Mbe et al. 2021]. The porosity is 17% then the number of pore space voxels is 22817013 voxels.

Figure 1 shows cross sections of the 3D binary image. Figure 2 shows a perspective view of the 3D binary image using Matlab routine.







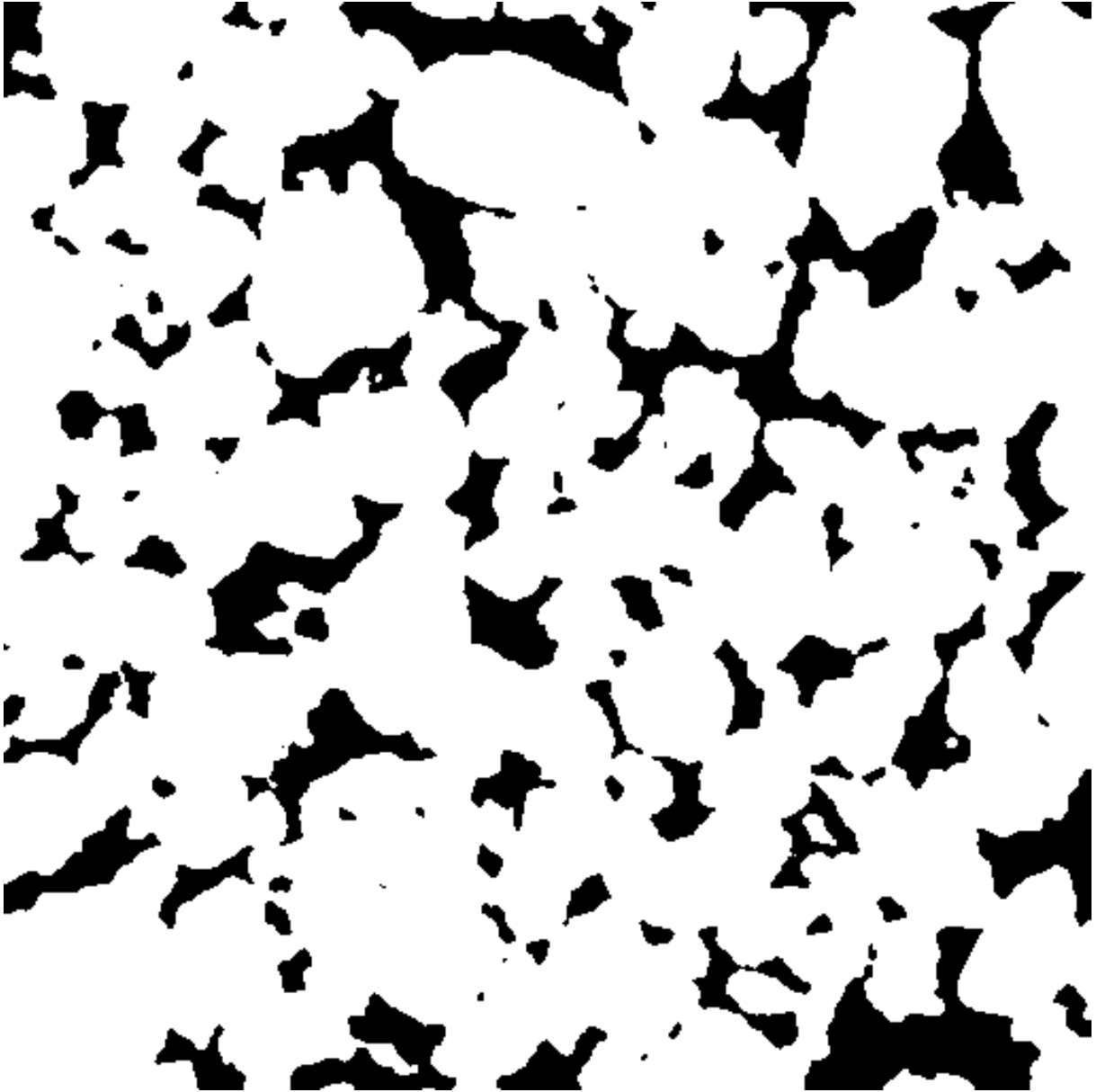


Figure 1: Cross sections of the 3D binary image representing pore space (pore space voxels are colored black)

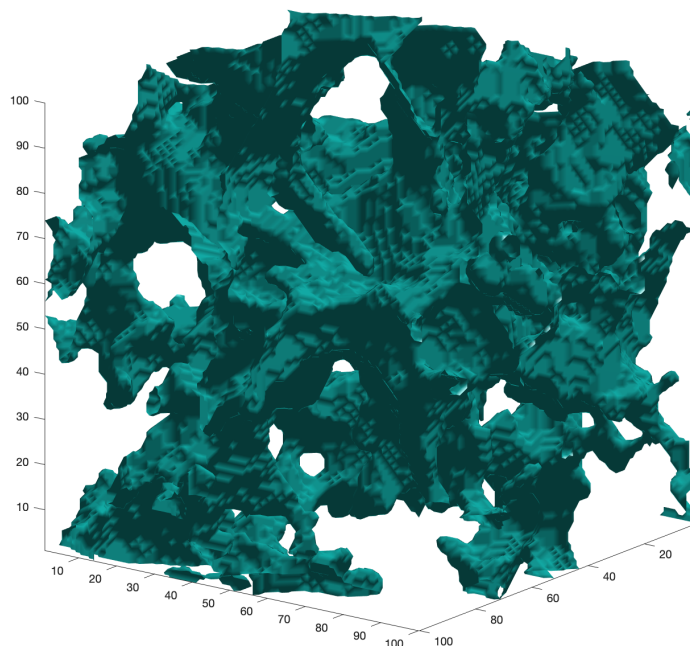


Figure 2: Perspective view of 3D pore space using Matlab routine (pore space is colored green)

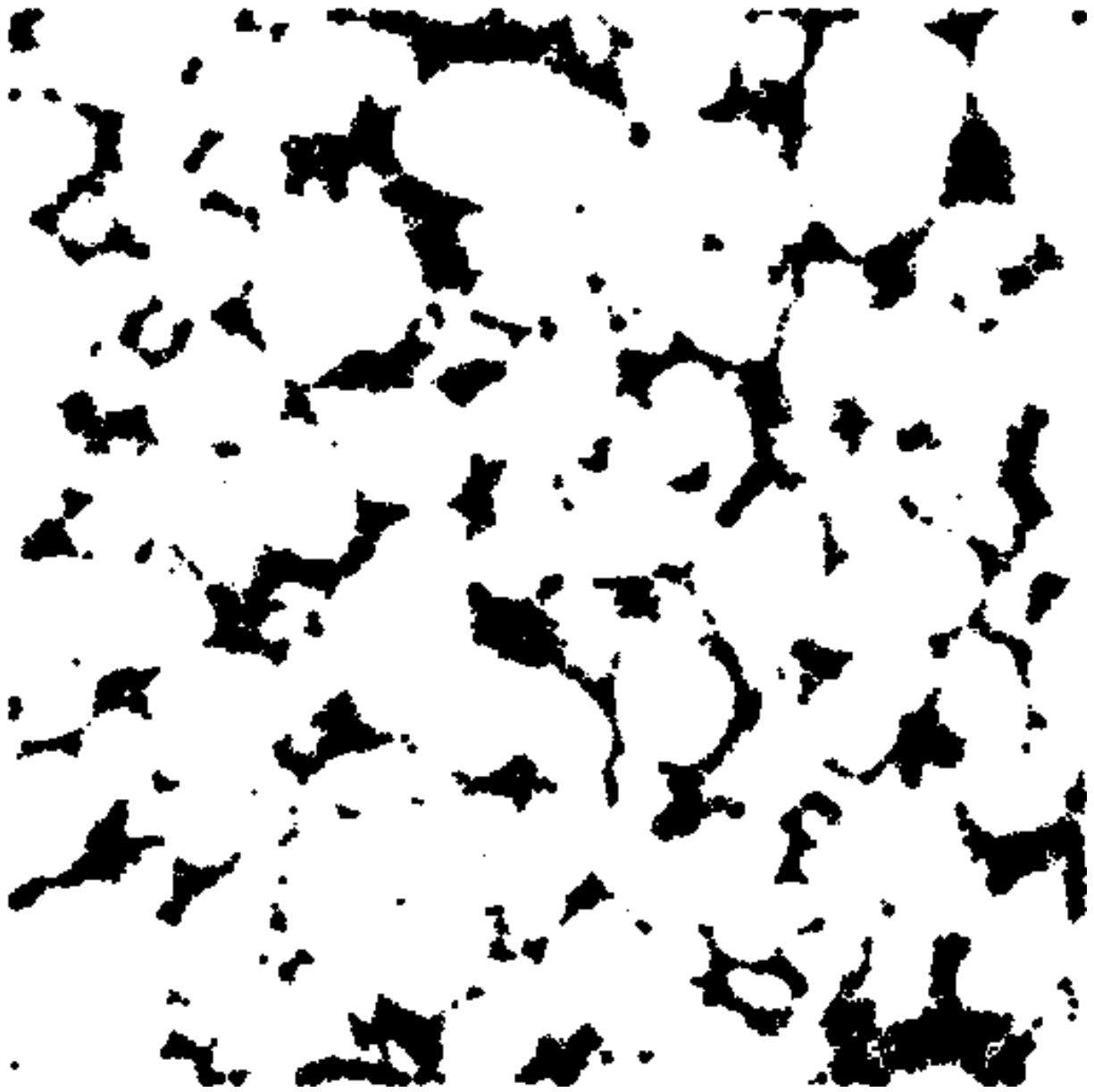
5.3 Pore space optimal ball network representation

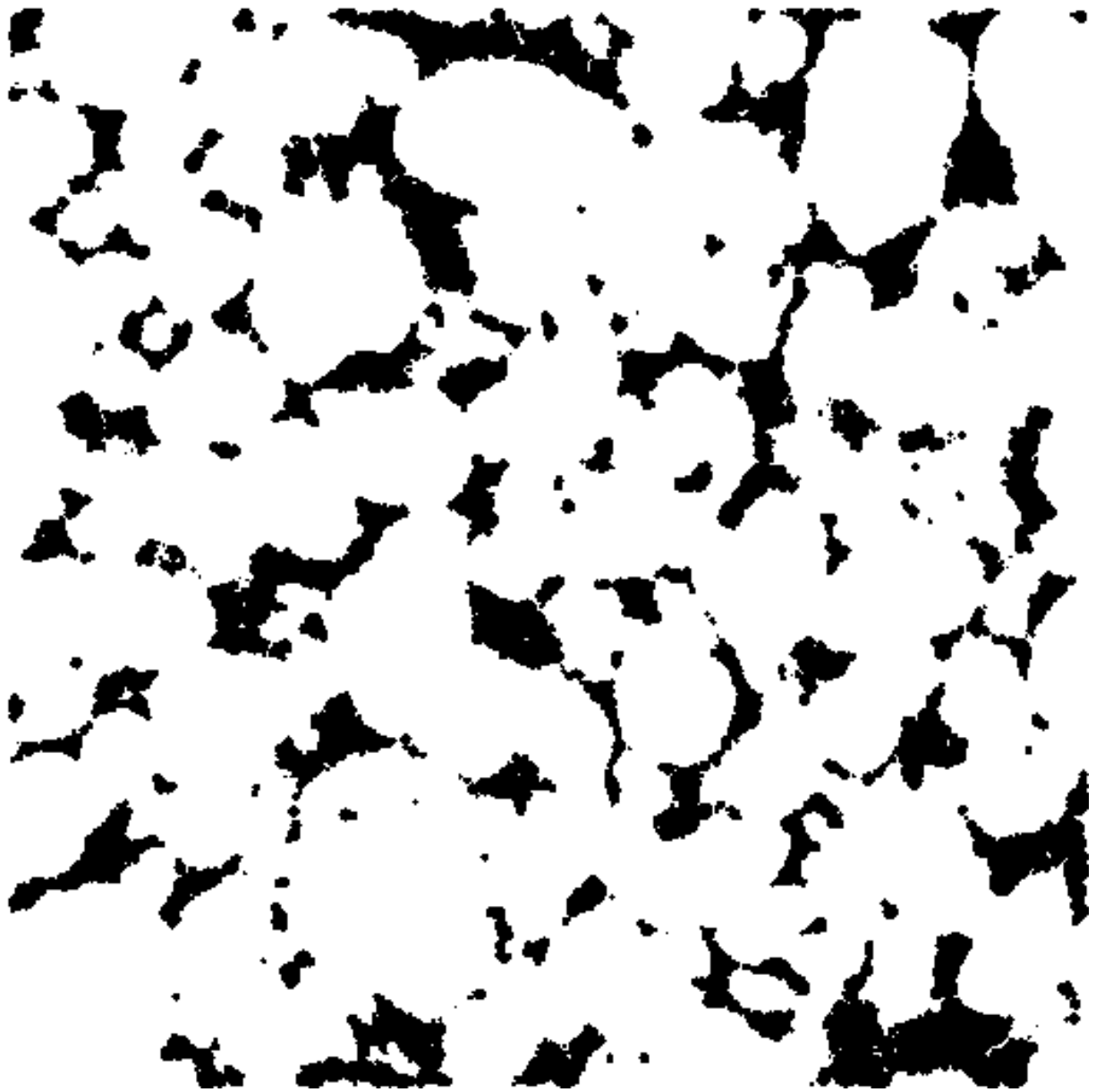
From initial voxel-based pore space representation, we extract the optimal ball network as described in [Monga et al. 2007]. The number of balls of the optimal network is 191583. Given that the number of pore space voxels is 22817013, we get a compacity ration up to 100 that is considerable for upcoming calculations. Figure 3-4 show cross sections of the ball network.

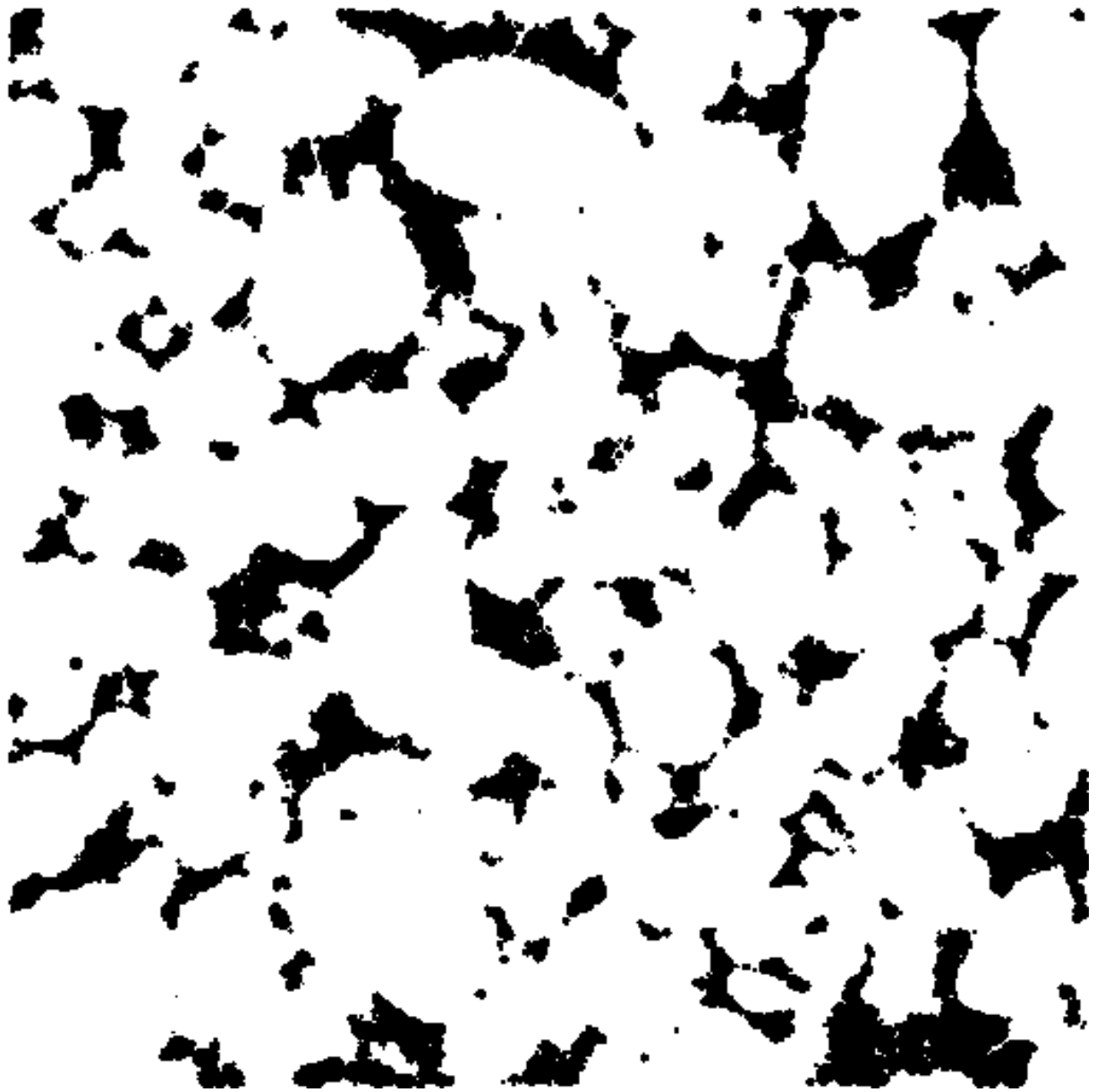
Figure 5-6 present perspective views of the optimal ball network using Matlab display routines.

In the sequel we perform the draining phase at different saturations (80%, 50%, 20%) using balls radiuses thresholding [Monga et al. 2007, Monga et al. 2008, Monga et al. 2014, Pot et al. 2015]. The principle is to select the balls whose radius is less than a given threshold. For each saturation we determine the threshold allowing to get the desired saturation (80%, 50%, 20%). For a saturation value of 100% we select all the balls (in our experience, the maximum

radius value is 18), the number of balls is 191583 (all the balls). For saturations 80%, 50%, 20% we get respectively (189127 balls, radius ≤ 16), (180498 balls, radius ≤ 13), (147654 balls, radius ≤ 9). For LBM method the draining phase is performed using the approach described in [Pot et al. 205].







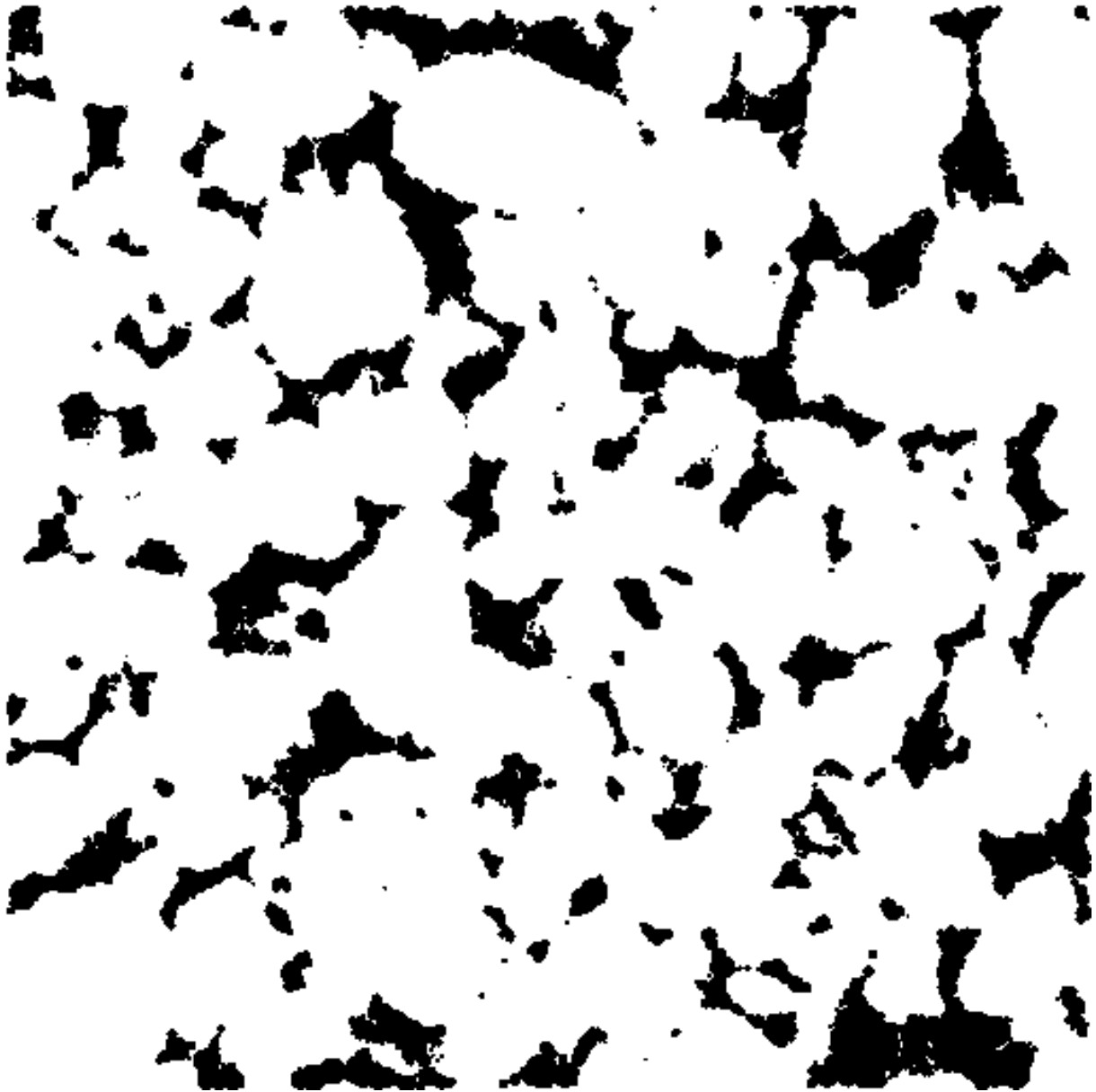
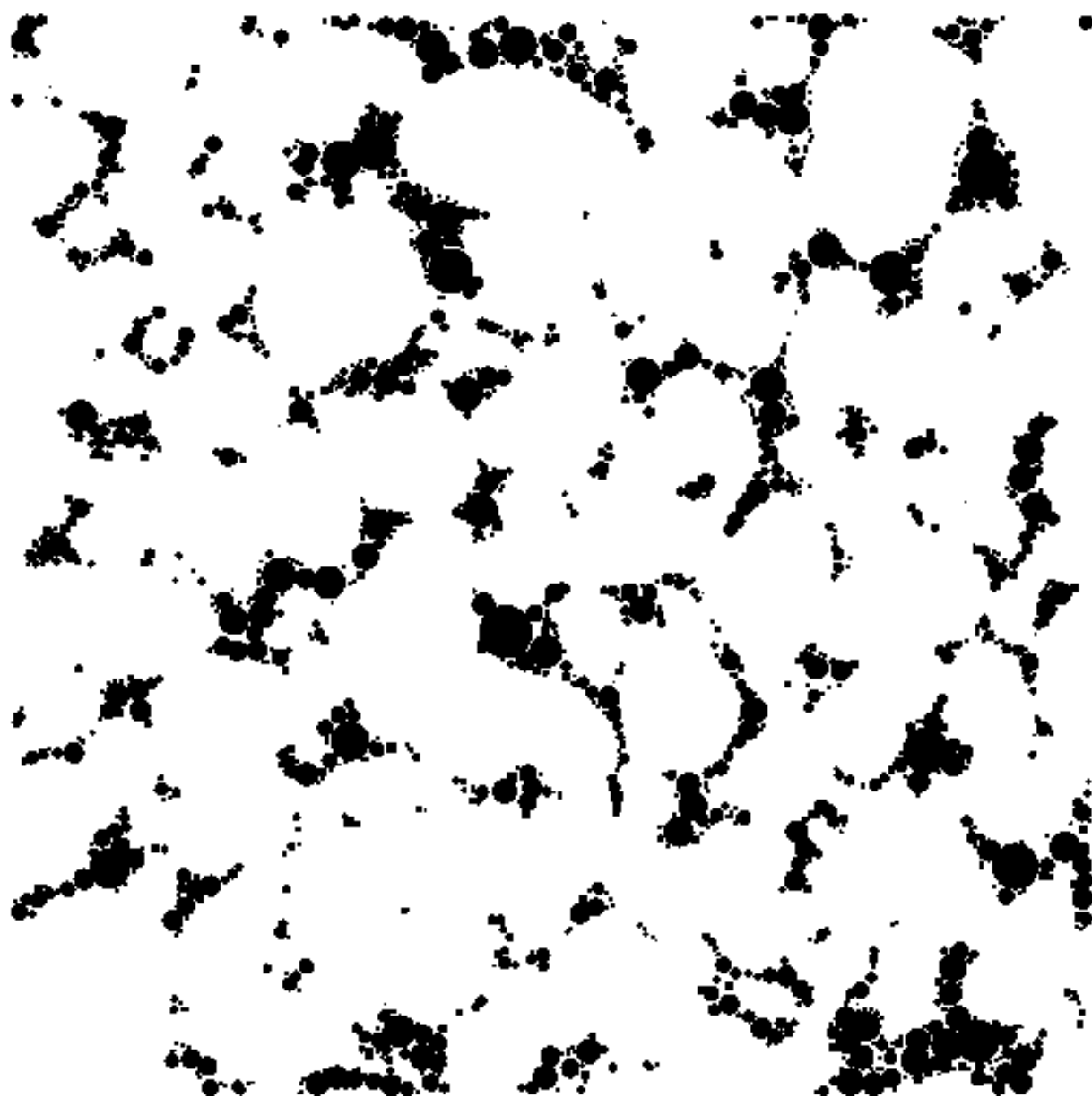
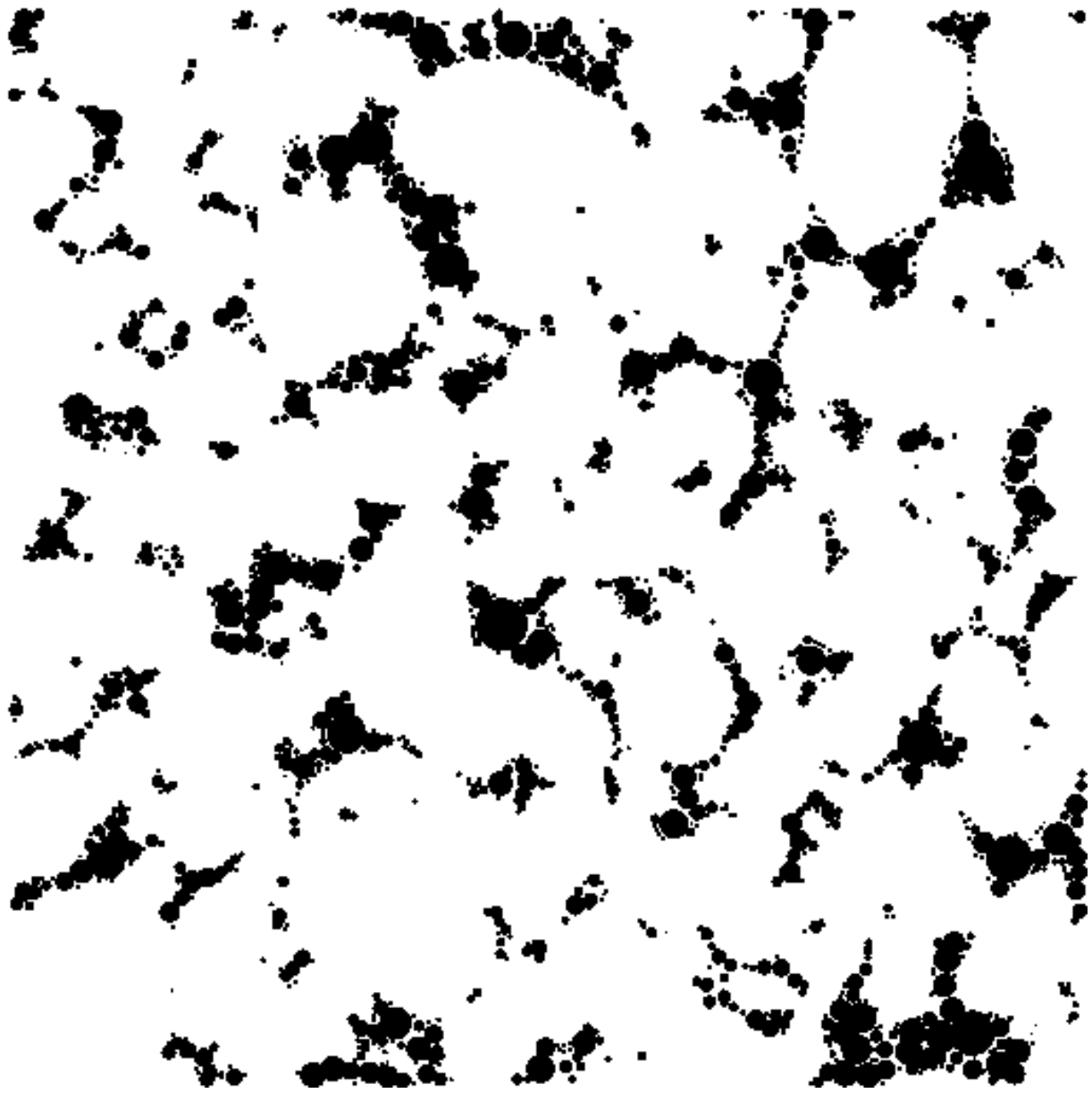
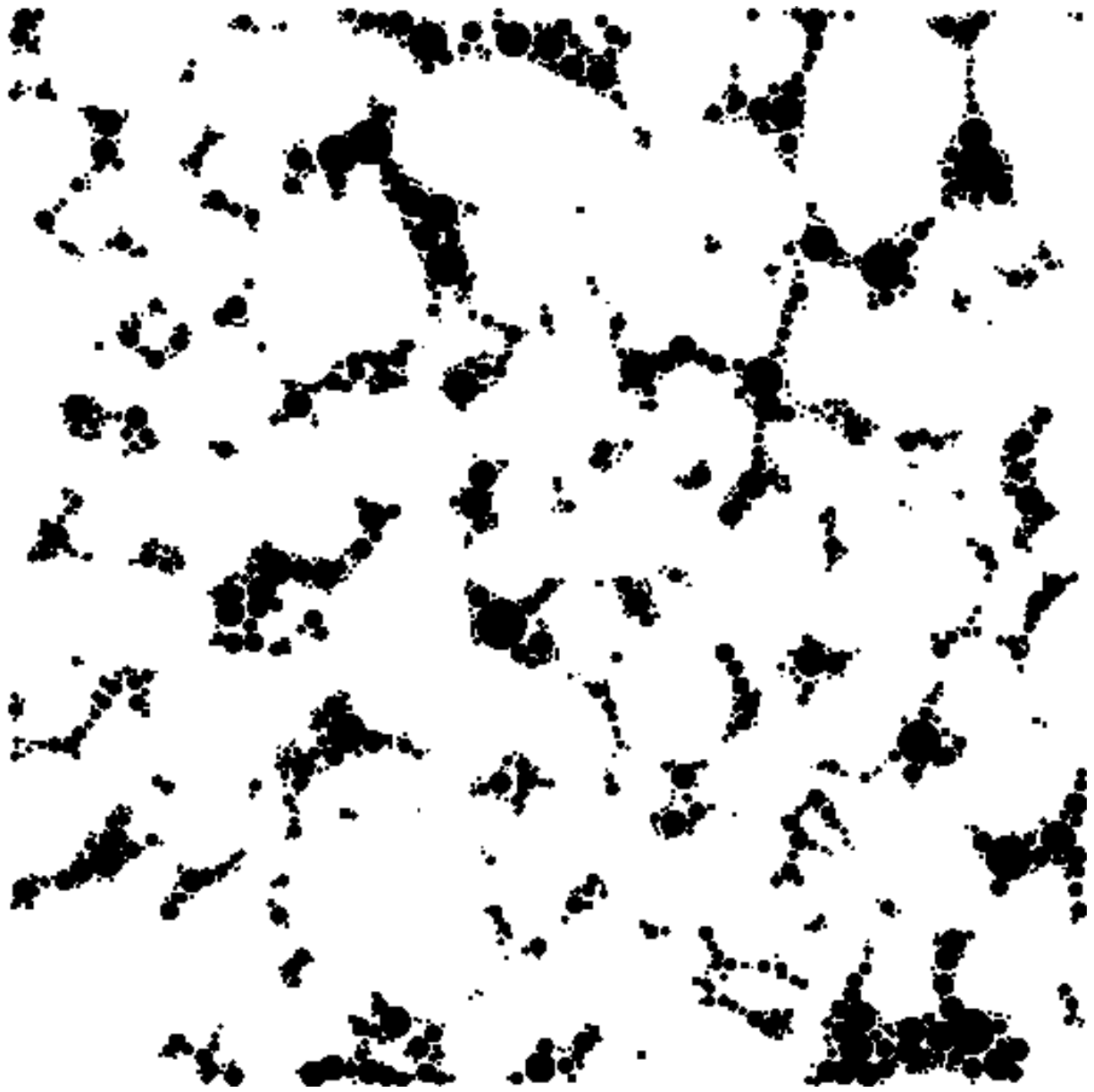


Figure 3: Cross sections of the ball network where the voxels of the balls are black colored (saturation 100%).







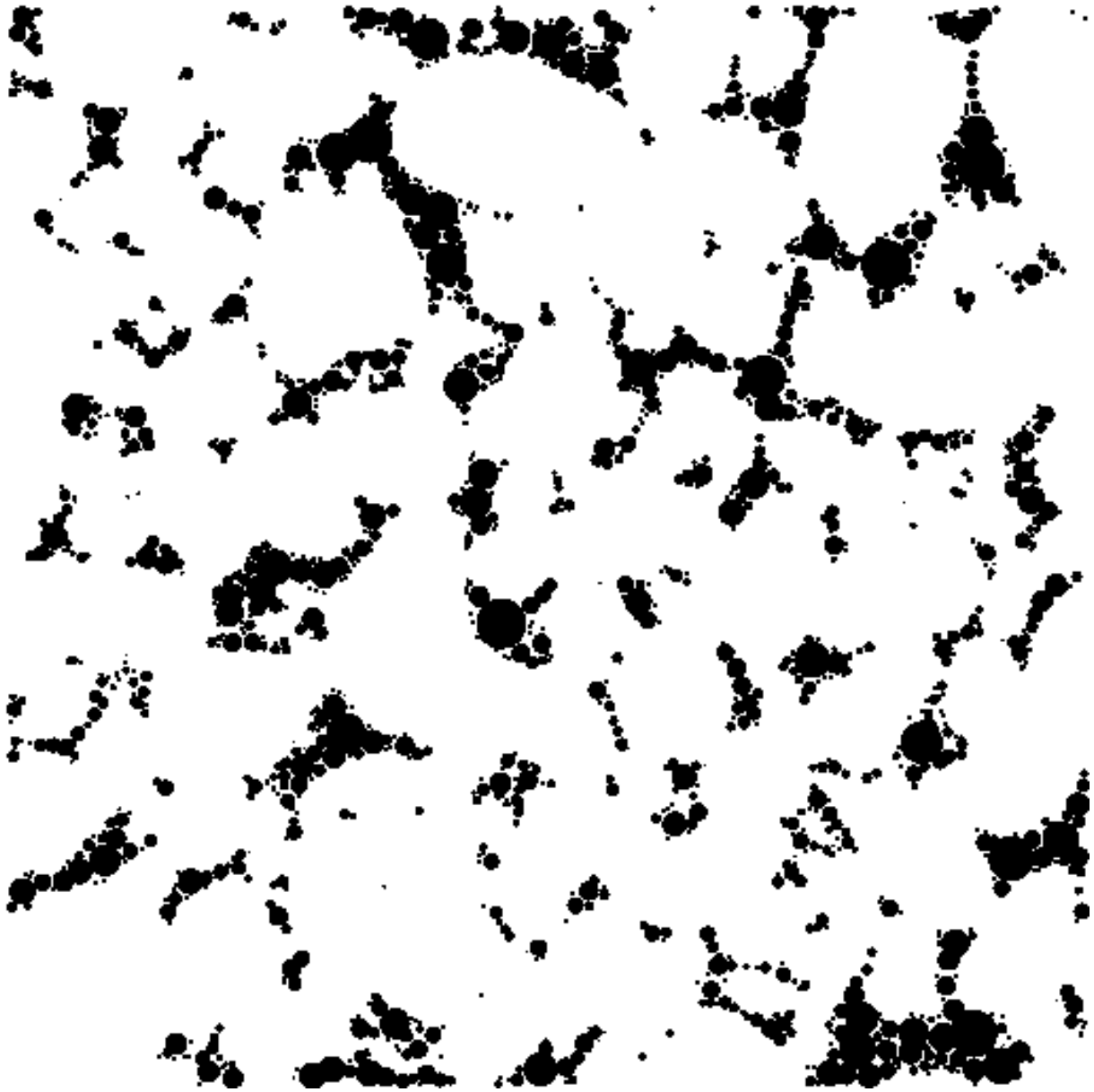


Figure 4: Cross sections of the ball network where the voxels of the balls are black colored.

We consider only the balls such the radius is at least 5 (saturation 100%)

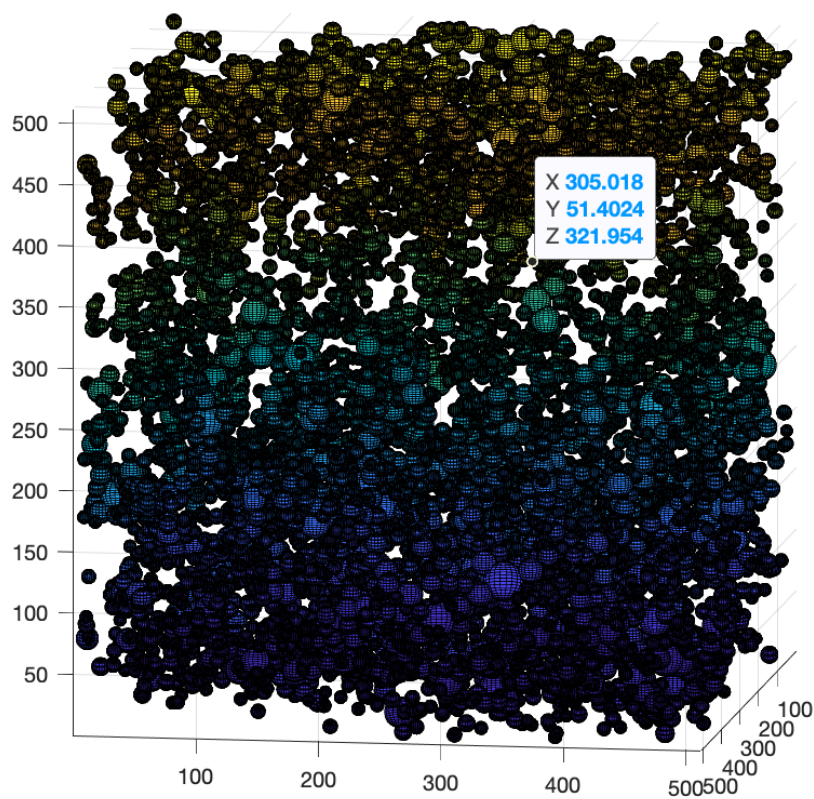


Figure 5: Perspective view of the balls whose radius is at least 5 (saturation 100%)

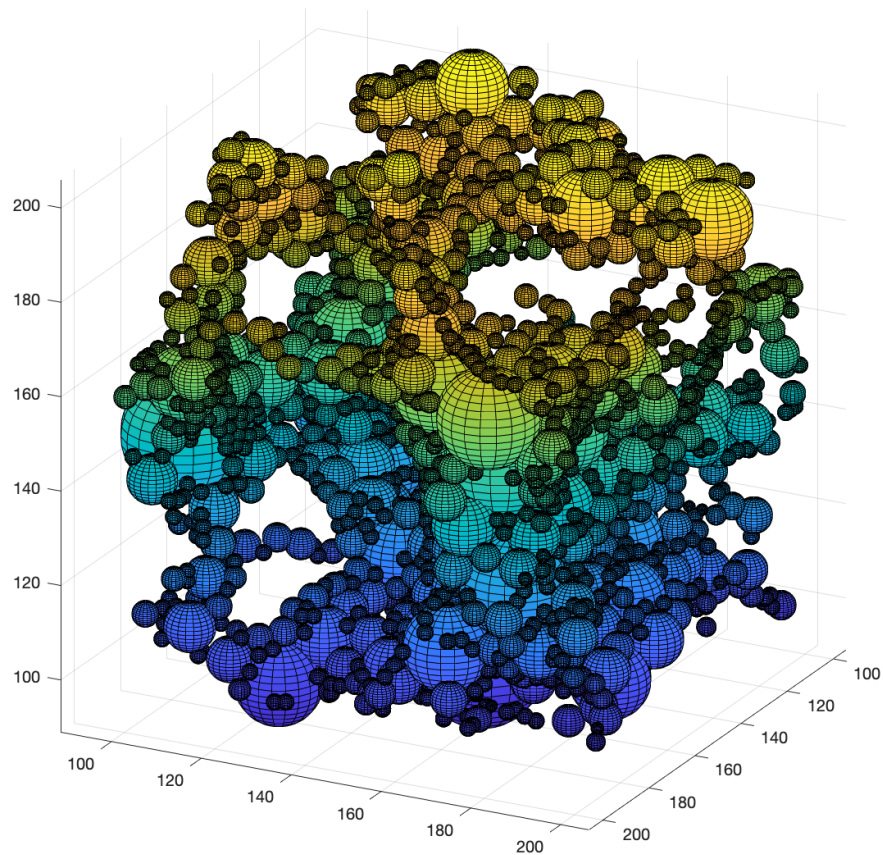


Figure 6: Zoom view of the ball network on 100x100x100 window in the center of the image (saturation 100%)

5.4 Diffusion coefficient calibration using Lattice Boltzman Method (LBM)

In this subsection, we compare the results, regarding numerical simulation of diffusion processes, provided by our approach (MOSAIC) and by LBM method. The basic principle of MOSAIC is to diffuse globally from one ball to the connected balls with respect to Fick laws. Therefore, even if the mathematical scheme is strictly the same for the two methods, MOSAIC will diffuse “faster” than LBM. That is the reason why, we need to calibrate the diffusion coefficient used for MOSAIC with the one of LBM. Unsurprisingly, the “MOSAIC diffusion

coefficient” is higher than the “LBM diffusion coefficient”, with a ratio around 2 that is reasonable. We calibrate MOSAIC diffusion coefficient using LBM diffusion coefficient in the case of 100% saturation (all the balls of the graph are considered). In next subsection, the microbial decomposition simulation results show that the ratio “LBM diffusion coefficient versus “MOSAIC diffusion coefficient” remains the same for other saturation values (80%, 50%, 20%).

In order to calibrate MOSAIC diffusion with LBM diffusion we use the following scheme.

We consider the first 300 planes ($z = \text{cste}$) of the $512 \times 512 \times 512$ image. We put, homogeneously, 592.7593 mg of carbon on the first two planes ($z = 0$ and $z = 1$). For LBM we consider all the voxels of the two planes ($z = 0$ and $z = 1$) and put $\frac{592.7593}{2 \times 512^2}$ mg of carbon in each voxel. For our approach MOSAIC, we consider all the balls intersecting the two first planes and put the total mass of carbon (592.7593 mg) proportionally to their volumes. Therefore, by construction the initial carbon concentration is the same in each ball intersecting the two first planes.

We simulate the diffusion using LBM for 1.783 hours. We set the diffusion coefficient to $6.73 \times 10^{-6} \text{ cm}^2 \text{ s}^{-1}$ that corresponds to the molecular diffusion coefficient of carbon (Dissolved Organic Matter, DOM) in water [Mbe et al. 2021]. For our specific image data and units, we get a diffusion coefficient around $C_1 = 100000 \text{ voxel}^2 \text{ j}^{-1}$. We measure the mass profile for each plane ($z = \text{cste}$) that is the total mass on each plane ($z=0, z=1, z=2, \dots, z=299$).

The simulation time of the diffusion is 1.783 hour.

In order to calibrate the value of the MOSAIC coefficient diffusion we match the two diffusion curves obtained with the two methods. The principle is to find out the MOSAIC diffusion coefficient corresponding to the LBM one ($C_1 = 100000 \text{ voxel}^2 \text{ j}^{-1}$). We minimize the inter-correlation (cosinus) between the two curves:

Let be the curve corresponding to LBM method when the diffusion coefficient is set to C_1 .

$L_{C_1}(i)$ is the total mass of DOM in plane number i . In our experiment $C_1 = 100000 \text{ voxel}^2 \text{ j}^{-1}$

Let $M_C(i)$ be the curve corresponding to MOSAIC method when the diffusion coefficient is set to C . We look for the optimal value of c such that $M_C(i)$ fits with $L_{C_1}(i)$.

We look for the value of c maximizing the intercorrelation (cosinus) between $M_c(i)$ and $L_{c_1}(i)$:

$$\cos(L_{C_1}, M_C) = \frac{L_{C_1} \cdot M_C}{\|L_{C_1}\| \|M_C\|} = \frac{\sum_{i=0}^{299} L_{C_1}(i) M_C(i)}{\sqrt{\sum_{i=0}^{299} L_{C_1}(i)^2} \sqrt{\sum_{i=0}^{299} M_C(i)^2}} \quad (26)$$

Figures 7,8,9 shows the comparison between L_{C_1} and M_C for $C = 60000, 48000, 40000$ (respectively). The optimal value for $\cos(L_{C_1}, M_C)$ is reached for $C = 40000$:

$\cos(L_{C_1}, M_{40000}) = 0.99$ (27). The difference between LBM and Mosaic curve near the origin is due to the fact that only a few balls intersect the first plane thus the initial DOM mass is more concentrated on the second plane. Figures 7,8,9 illustrate our calibration scheme.

Thus, in the sequel, we set the MOSAIC diffusion coefficient to $C = 40000$

The next subsection deals with the comparison MOSAIC versus LBIOS for microbial decomposition simulation.

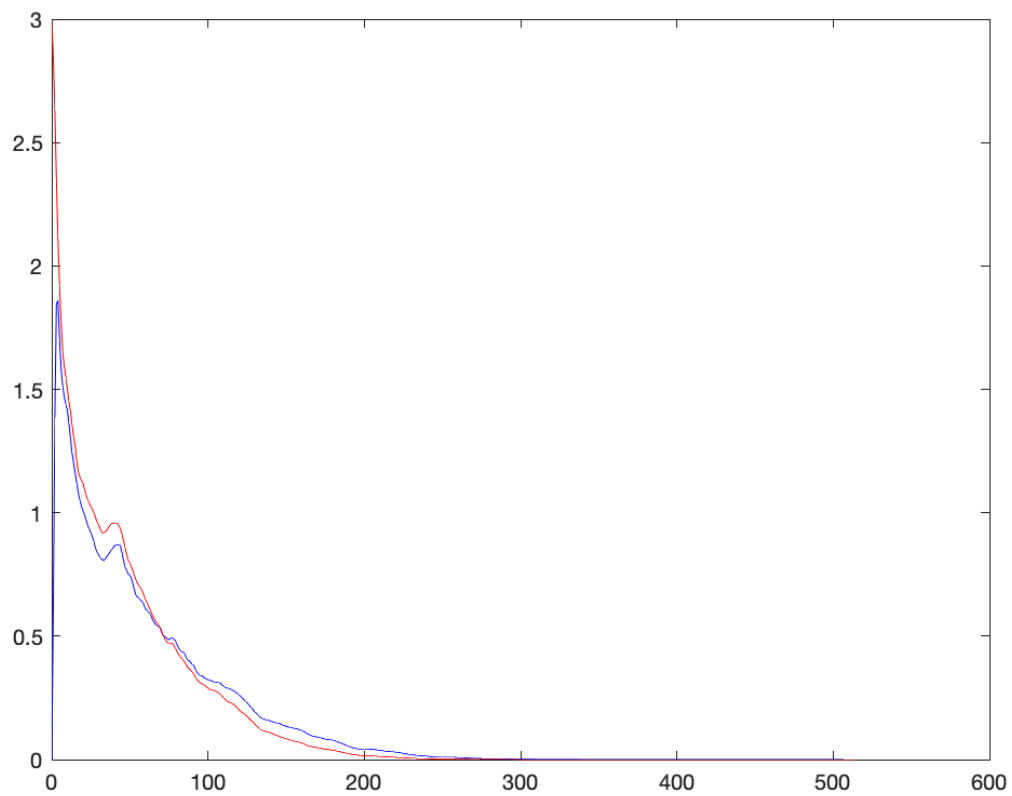


Figure 7: Comparison of the diffusion simulation results MOSAIC/LBIOS ; MOSAIC curve is blue colored ; LBIOS curve is red colored ; LBIOS diffusion coefficient is set to 100000 ; MOSAIC diffusion coefficient is set to 60000

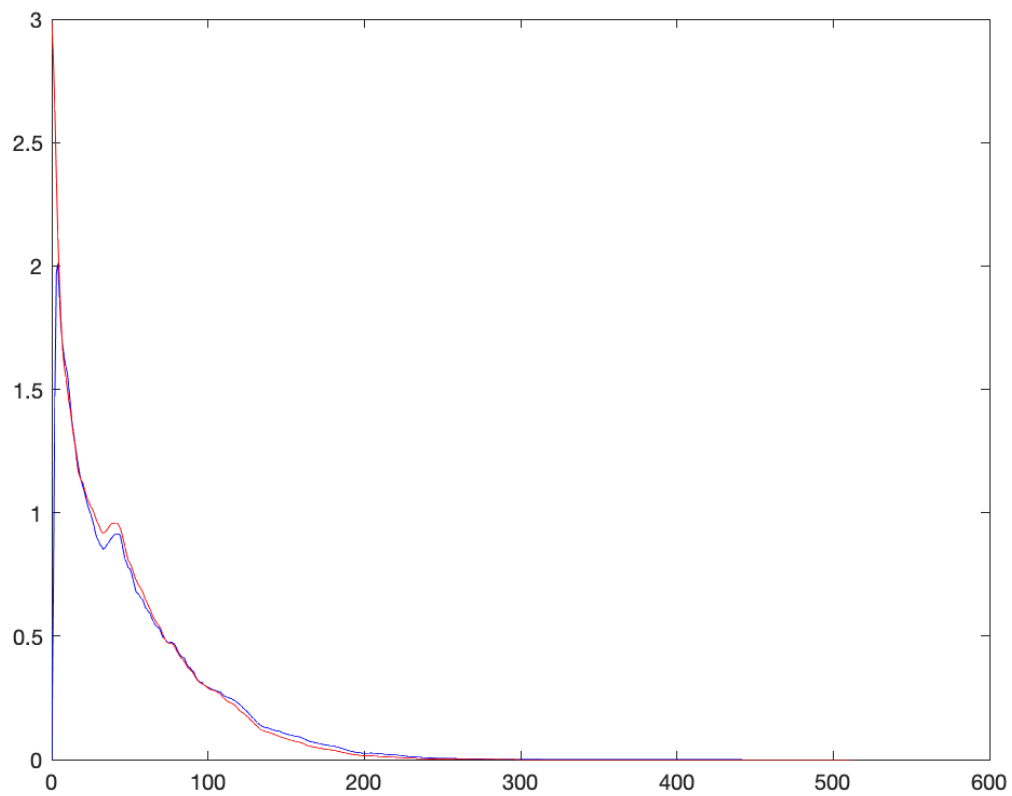


Figure 8: Comparison of the diffusion simulation results MOSAIC/LBIOS ; MOSAIC curve is blue colored ; LBIOS curve is red colored ; LBIOS diffusion coefficient is set to 100000 ; MOSAIC diffusion coefficient is set to 48000

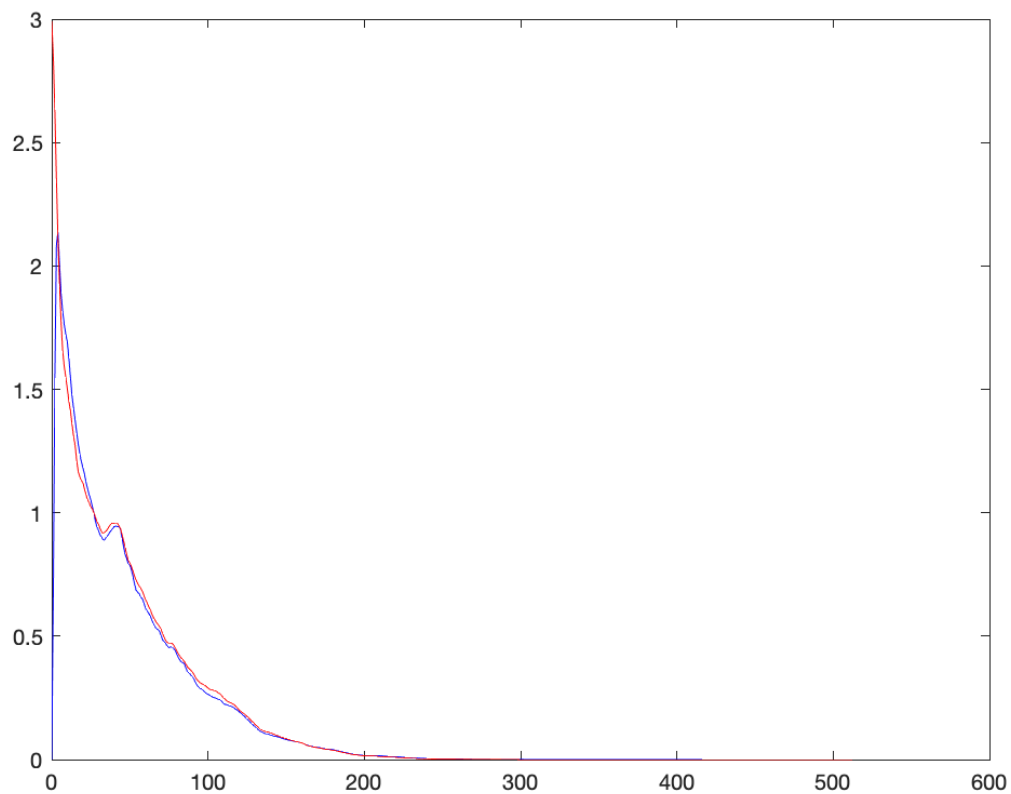


Figure 9: Comparison of the diffusion simulation results MOSAIC/LBIOS ; MOSAIC curve is blue colored ; LBIOS curve is red colored ; LBIOS diffusion coefficient is set to 100000 ; MOSAIC diffusion coefficient is set to 40000 ; The normalized intercorrelation between the two curves is 0.99.

5.5 Microbial decomposition simulation: comparison with LBM

This section tackles the validation of MOSAIC approach by comparison with LBM method. The experimental scheme was the following. We performed numerical simulation of microbial decomposition with LBM and MOSAIC on strictly same data set [Mbe et al.]. We show that the outputs of the two methods are very close (see figures 10,11,12). The computing time, on a

regular PC station, is about 3 weeks for LBM and 15-30 minutes for MOSAIC (implicit numerical scheme). The geometrical modeling stage of MOSAIC, which have to run only once, takes about 20 minutes CPU (see section 5.3). We took for LBM the diffusion coefficient of carbon in water as mentioned in the previous section ($100000 \text{ voxel}^2 \text{ j}^{-1}$). We took for MOSAIC the calibrated diffusion coefficient as defined in the previous section ($40000 \text{ voxel}^2 \text{ j}^{-1}$). We make running the numerical simulation of the microbial decomposition for four saturation values (100%, 80%, 50%, 20%). For MOSAIC, the draining phase was performed thanks to the ball network as described in section 5.3 that is also much more faster than the voxel-based draining in LBM.

The biological parameters of Monga et al. (2014) from *Arthrobacter* sp. 9R were taken [Mbe et al. 2021]:

ρ the relative respiration rate was set to 0.2 j^{-1} , μ the relative mortality rate was set to 0.5 j^{-1} , ρ_m the proportion of MB (Microbial Mass) returning to DOM (Dissolved Organic Matter) was set to 0.55 (the other part returns to SOM), v_{FOM} and v_{SOM} the relative decomposition rates of FOM and SOM were respectively set to 0.3 j^{-1} and 0.01 j^{-1} , v_{DOM} the maximum relative growth rate of MB was set to 9.6 j^{-1} , κ_b the constant of half saturation of DOM was set to 0.001 gCg^{-1} .

The initial distribution of the masses of MB and DOM was done as follows.

We put homogeneously 0.2895 mg of DOM within the pore space. For LBM it was put homogeneously in the voxels filled with water after draining. For MOSAIC it was put homogeneously (in the sense of concentration) in the balls filled with water after draining.

Regarding the microorganisms, we put 1000 spots of bacteria distributed in the pore space (filled with water). For LBM we distributed the amount of bacteria ($5.2 \cdot 10^7$ bacteria = $2 \cdot 10^{-12}$ $5.2 \cdot 10^7$ g) in the voxels filled with water. For MOSAIC we put the same amount of bacteria in the balls intersecting the voxels filled with bacteria in the LBM scheme.

Therefore, the distributions of microorganisms and of organic matter is as close as possible for the two models (LBM and MOSAIC). Of course, given that the pore space description is based on voxels for LBM and on geometrical primitives (balls) for MOSAIC, the distributions cannot be strictly identical. We kept the same mass of DOM whatever the water content and the soil density, which implies that the concentrations increased when the water saturations decreased.

Thus, our experimental scheme allowed to compare rigorously the numerical simulation of the microbial decomposition (including organic matter diffusion) provided by the two methods (LBM and MOSAIC). We realized the comparison for four values of water saturation: 100%, 80%, 50%, 20% by keeping strictly the same parameters for the two methods. The real simulation time was five days. The computing time was 15-20 minutes CPU for MOSAIC and several weeks for LBM. The good concordance of the curves showing the biological dynamics (see figures 10 to 13), illustrates the pertinence and effectiveness of our approach. The two methods have a computational complexity proportional to the simulation time. MOSAIC complexity is also proportional to the number of arcs of the geometrical primitives graph. LBM complexity is proportional to the size of the voxel mesh describing the pore space.

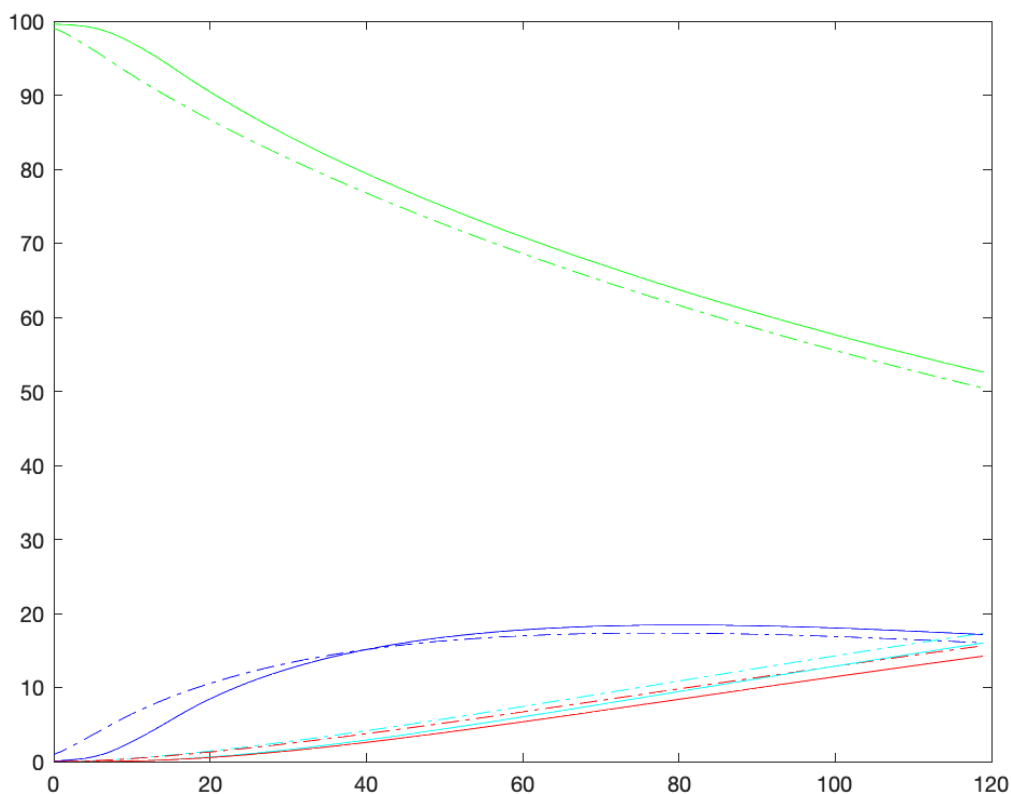


Figure 10: Comparison of LBM and MOSAIC biological dynamics curves when saturation is set to 100% ; LBM curves are dotted lines and MOSAIC curves solid lines ; X-axis represents time expressed in hour unit (5 days = 120h) ; Y-axis represents masses expressed in percentage of the total initial mass ; the mass of Dissolved Organic Matter (DOM) corresponds to green colored curves ; the Microbial Mass (MB) corresponds to dark blue colored curves; CO₂ gas mass corresponds to red colored curves : Solid Organic Matter (SOM) mass corresponds to light blue

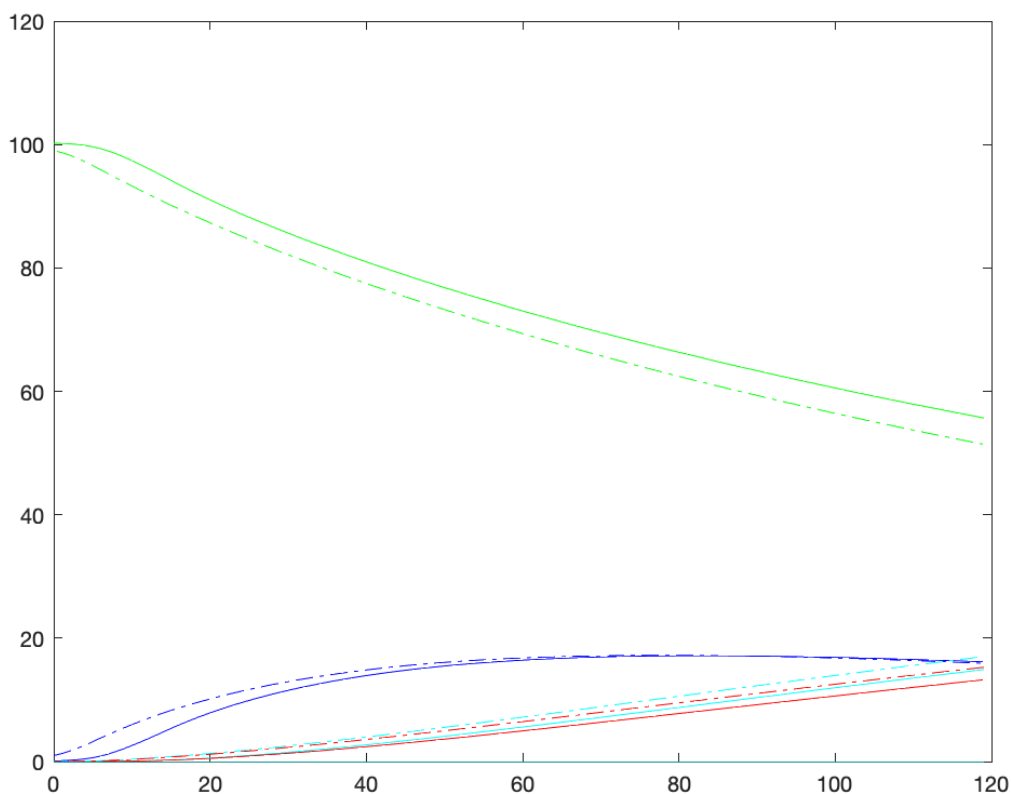


Figure 11: Comparison of LBM and MOSAIC biological dynamics curves when saturation is set to 80% ; LBM curves are dotted lines and MOSAIC curves solid lines ; X-axis represents time expressed in hour unit (5 days = 120h) ; Y-axis represents masses expressed in percentage of the total initial mass ; the mass of Dissolved Organic Matter (DOM) corresponds to green colored curves ; the Microbial Mass (MB) corresponds to dark blue colored curves; CO₂ gas mass corresponds to red colored curves : Solid Organic Matter (SOM) mass corresponds to light blue

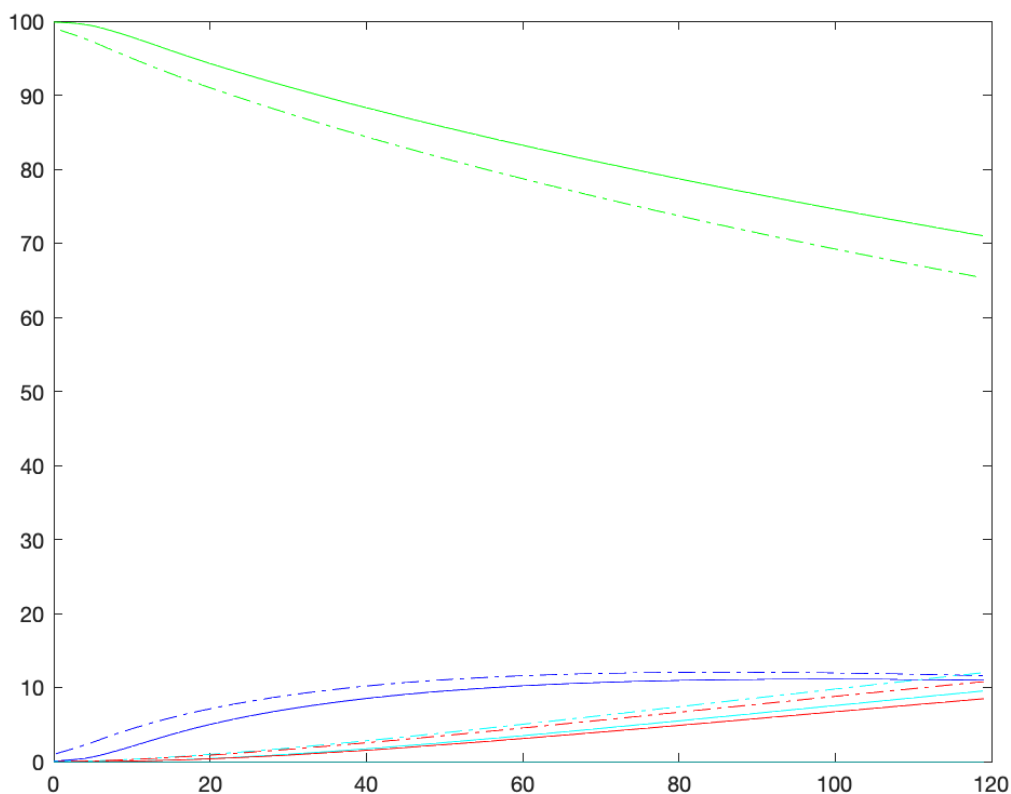


Figure 12: Comparison of LBM and MOSAIC biological dynamics curves when saturation is set to 50% ; LBM curves are dotted lines and MOSAIC curves solid lines ; X-axis represents time expressed in hour unit (5 days = 120h) ; Y-axis represents masses expressed in percentage of the total initial mass ; the mass of Dissolved Organic Matter (DOM) corresponds to green colored curves ; the Microbial Mass (MB) corresponds to dark blue colored curves; CO₂ gas mass corresponds to red colored curves : Solid Organic Matter (SOM) mass corresponds to light blue

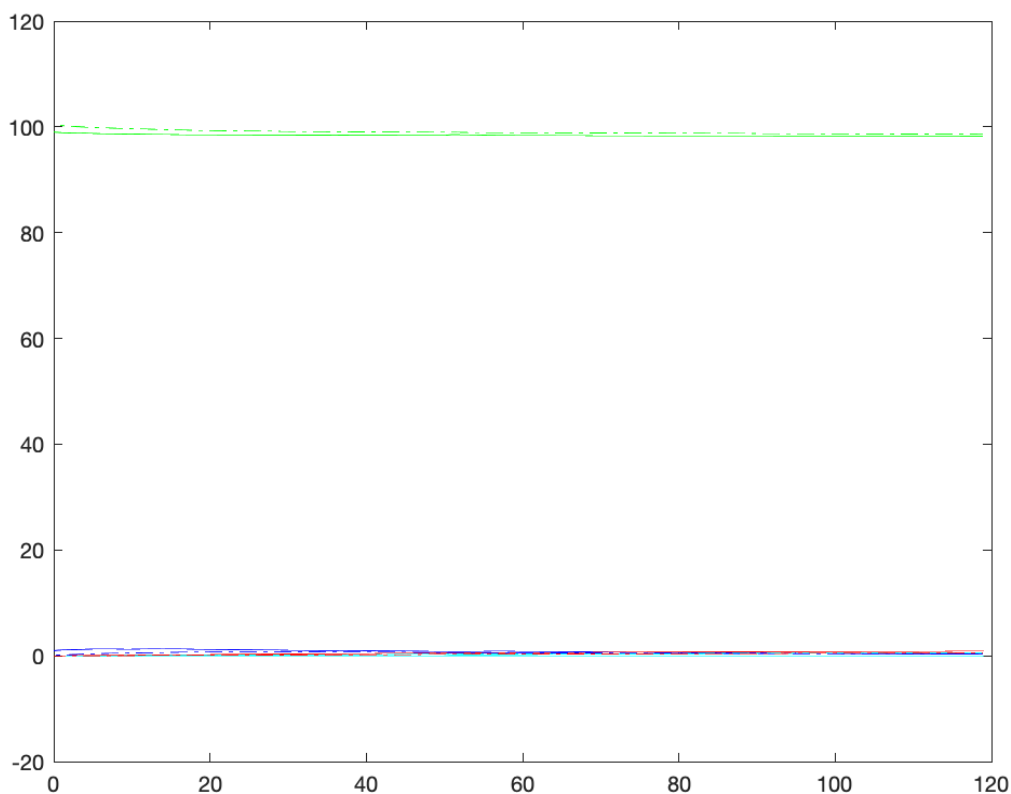


Figure 13: Comparison of LBM and MOSAIC biological dynamics curves when saturation is set to 20% ; LBM curves are dotted lines and MOSAIC curves solid lines ; X-axis represents time expressed in hour unit (5 days = 120h) ; Y-axis represents masses expressed in percentage of the total initial mass ; the mass of Dissolved Organic Matter (DOM) corresponds to green colored curves ; the Microbial Mass (MB) corresponds to dark blue colored curves; CO₂ gas mass corresponds to red colored curves : Solid Organic Matter (SOM) mass corresponds to light blue

5.6 Microbial decomposition simulation over long period

The considerable gain, regarding computational cost, opens important methodological new perspectives. Also we point out that the results presented here are provided using a regular and common PC (2.8 GHz, Intel Core i7, 4 computer cores).

Indeed, the main possibilities allowed by this computational jump are:

- we can run the numerical simulation using data images of bigger size that will be a key point for upscaling issue ;
- the real simulation time can be increased, below we present results obtained for a one month period that we could practically not get using classical approaches like LBM
- we can test more easily accessibility criteria (of the organic matter by the microorganisms) conditioning the biological dynamics as initiated in [Mbe et al. 2021]
- we can simulate more complex scenarios for instance including several microorganisms species
- thanks to MOSAIC approach based on geometrical primitives, we can take into account deformations of the pore space during the microbial decomposition process

This subsection illustrates the second point that is the use of longer (real) simulation period.

We considered the scenario where the total initial mass of organic matter (DOM) is concentrated within a single ball (0.2895 mg). The saturation has been set to 100% . Same as in the previous scenario the microorganisms are put in 1000 spots ($5.2 \cdot 10^7$ bacteria = $2 \cdot 10^{-12}$ $5.2 \cdot 10^7$ g). We performed the microbial decomposition simulation for four different initial positions of the patch of DOM.

As expected, the biological dynamics depends on the initial position of the organic matter patch with respect to microorganisms. Also, after one month, the diffusion process has brought all DOM to the microorganisms.

We point out that such numerical simulation using classical voxel based methods like LBM would take about 6 months computing time instead of 3-4 hours with MOSAIC approach.

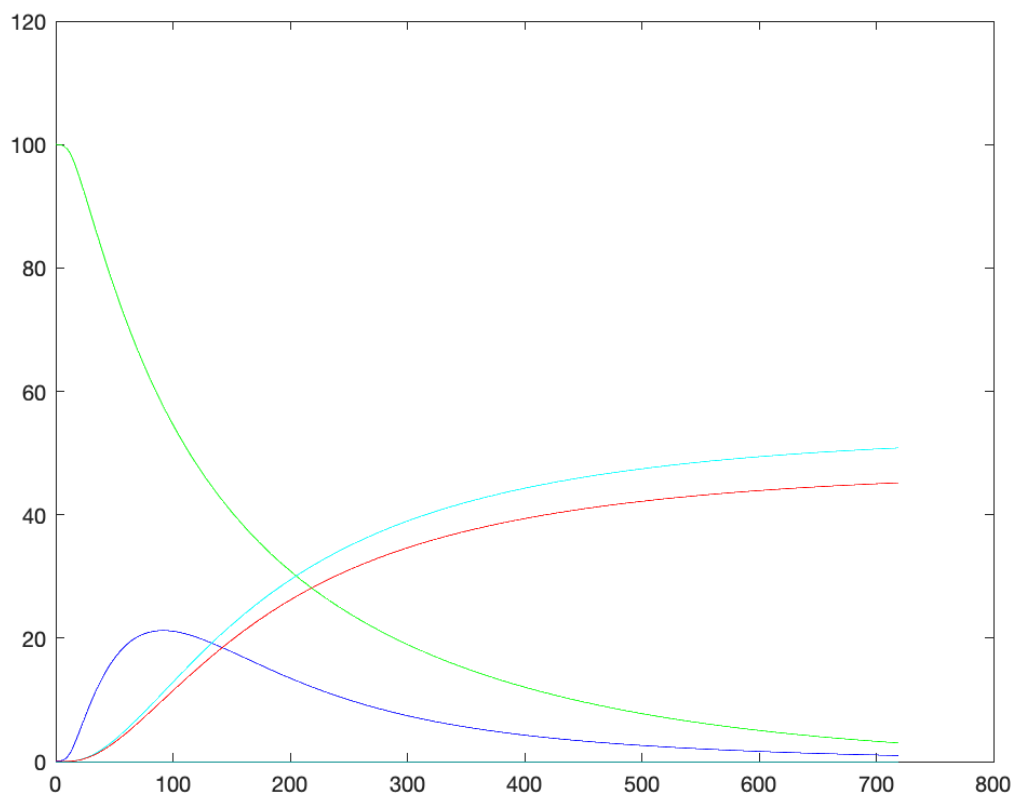


Figure 14: X-axis represents time expressed in hour unit (30 days = 720h) ; Y-axis represents masses expressed in percentage of the total initial mass ; the mass of Dissolved Organic Matter (DOM) corresponds to green colored curves ; the Microbial Mass (MB) corresponds to dark blue colored curves; CO₂ gas mass corresponds to red colored curves : Solid Organic Matter (SOM) mass (coming from MB degradation) corresponds to light blue

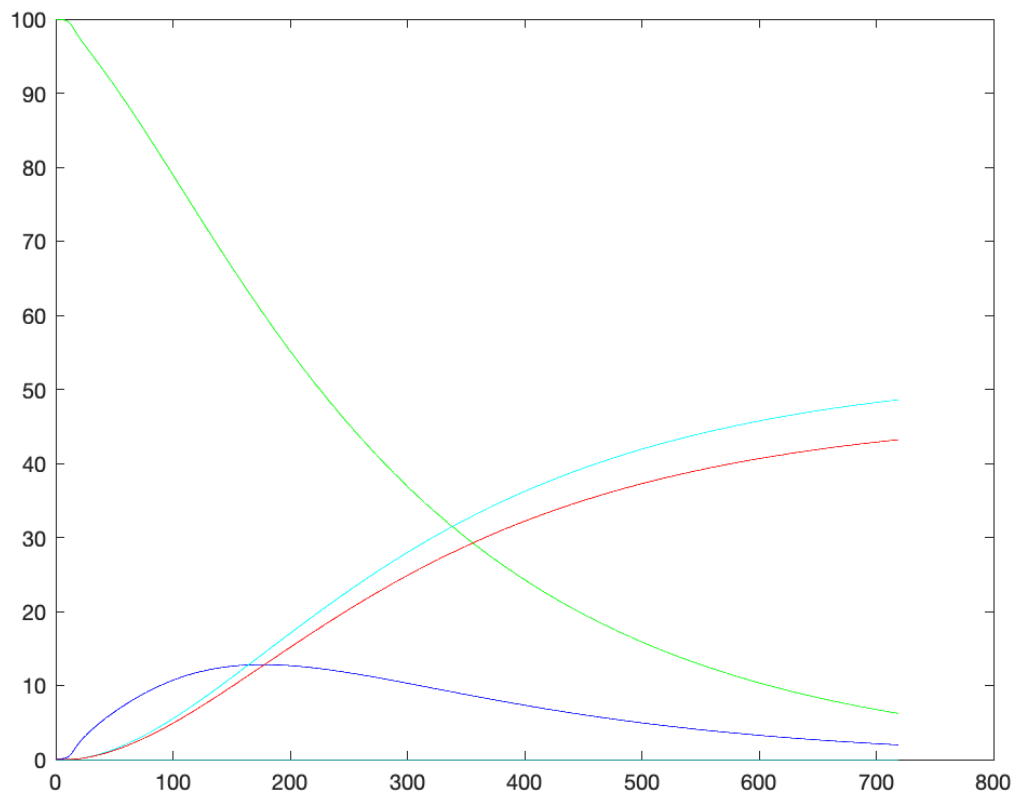


Figure 15: Same as figure 14 for another initial position of the DOM patch

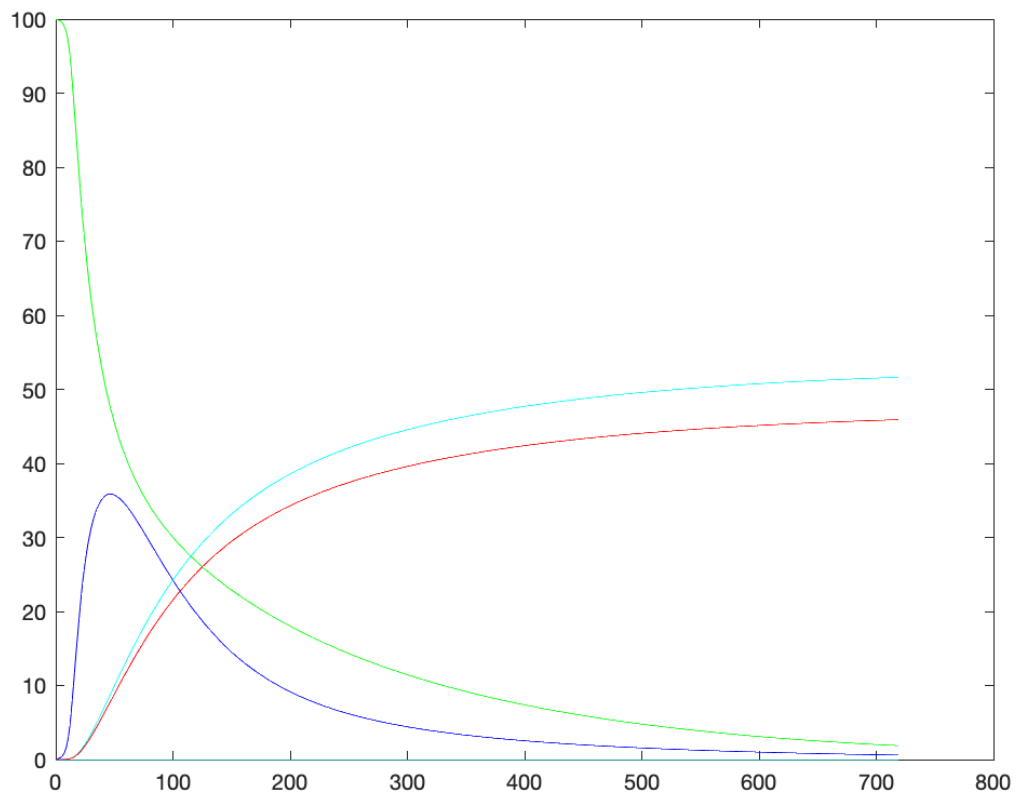


Figure 16: Same as figure 15 for another initial position of the DOM patch

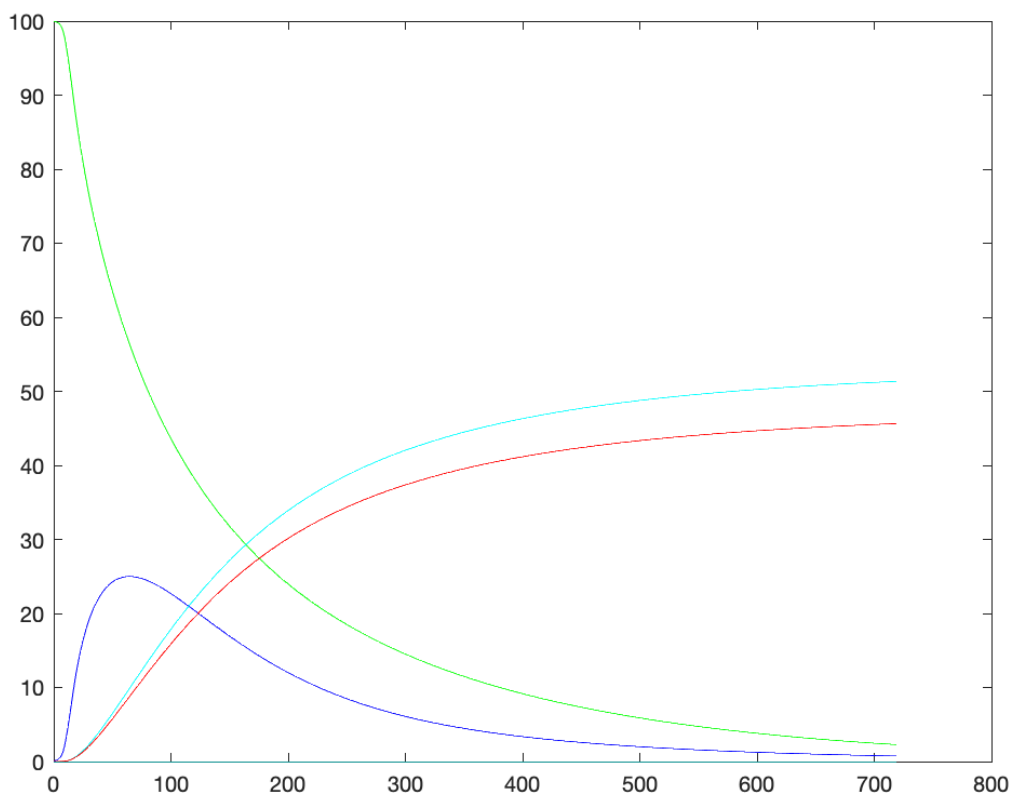


Figure 17: Same as figure 16 for another initial position of the DOM patch

6-Conclusion

This paper describes the mathematical and algorithmic framework of [Mbe et al. 2021].

This work follows the one described in [Monga et al. 2014]. In this previous study, we proposed to simulate microbial decomposition using a graph of geometrical primitives representing the pore space. The principle was to compute an intrinsic piecewise approximation of pore space by means of advanced computer vision algorithms [Monga et al. 2007, Monga 2007, Ngom et al. 2011]. Afterward, we represented the set of geometrical primitives (tangent or disjoint two by two) using an attributed relational graph. The simulation of microbial decomposition was then reduced to graph updating [Monga et al. 2014, Monga et al. 2008, Monga et al. 2009].

In the present work, we propose a formalization for numerical simulation of biological dynamics within complex geometric shapes. We come up with a generic algorithmic tool which

can be used for numerical simulation of most microbial decomposition processes from high resolution CT images. The basic idea consists in expressing biological dynamics as transformation and diffusion processes in the graph representing pore space. Regarding the numerical simulation of diffusion processes, we propose an implicit numerical scheme that is much more efficient than the explicit one used in [Monga et al; 2014]. Thanks to this implicit numerical scheme, the computational complexity has been significantly reduced (up to a ratio of 30). We validate our approach by comparing the results with the ones provided by classical Lattice Boltzmann Model (LBM). Compared to LBM we decreased the computing time with a ratio of about 1000 that is considerable, even if the results are normally slightly less precise. An extensive set of simulations are presented to validate our approach on distinct experiments.

Acknowledgments

The research described in this article was made possible through NPRP grant #9-390-1-088 from the Qatar National Research Fund. We thank Mouhad Klai and Philippe Baveye for helping to improve the manuscript and for stimulating discussions.

References

Bultreys T, Van Hoorebeke L, Veerle C. Multi-scale, 2015. Micro-computed tomography-based pore network models to simulate drainage in heterogeneous rock. *Advances in Water Resources* 2015;78 :36-49

H.M Byrne, T Alarcon, M.R Owen, S.D Webb and P.K Maini, 2006. Modelling aspects of cancer dynamics: a review. *Philosophical Transactions of the Royal Society*.

Volume 364 Issue 1843

Ayaz M, Maša P., 2014. The effect of microporosity on transport properties in porous media. *Advances in Water Resources* ; Vol 63 :104–119

Philippe C. Baveye, Wilfred Otten, Alexandra Kravchenko, María Balseiro Romero, Éléonore Beckers, Maha Chalhoub, Christophe Darnault, Thilo Eickhorst, Patricia Garnier, Simona Hapca, Olivier Monga, Carsten Müller, Naoise Nunan, Valérie Pot, Steffen Schlüte, Hannes Schmidt, Hans-Jörg Vogel, 2018. Emergent properties of microbial activity in heterogeneous soil microenvironments: Different research approaches are slowly converging, yet major challenges remain. *Frontiers in Microbiology*, *Front. Microbiol.* 8:1364. doi: 10.3389/fmicb.2017.01364.

Hidde de Jong, 2004. Modeling and Simulation of Genetic Regulatory Systems: A Literature Review. *Journal of Computational Biology*, Vol. 9, No. 1

Genty, A., & Pot, V. (2013). Numerical simulation of 3D liquid-gas distribution in porous media by a two-phase TRT Lattice Boltzmann method. *Transport in Porous Media*, 96, 271-294, Doi: 10.1007/s11242-012-0087-9

Genty, A., & Pot, V. (2014). Numerical calculation of effective diffusion in unsaturated porous media by the TRT Lattice Boltzmann method. *Transport in Porous Media*, 105, 391-410, Doi: 10.1007/s11242-014-0374-8

Kolade M., Owolabi, Kailash C., Patidar 2016. Numerical simulations of multicomponent ecological models with adaptive methods. *Theoretical Biology and Medical Modelling*, volume 13, Article number: 1

V Pot, S Peth, O Monga, L Vogel, A Genty, P Garnier, L Vieublé-Gonod, M Ogurreck, F Beckmann, P Baveye, 2015. Three-dimensional distribution of water and air in soil pores: Comparison of two-phase two-relaxation-times lattice-Boltzmann and morphological model outputs with synchrotron X-ray computed tomography data. *Advances in Water Resources* ;84 : 87–102

O Monga, N Ngom, J F Delerue, 2007. Representing geometric structures in 3-D tomography soil images: Application to pore space modelling. *Computers and Geosciences* ; Vol. 33 : 1140–1161

O Monga, P Garnier, V Pot, E Coucheney, N. Nunan, W Otten and C Chenu, 2014. Simulating microbial degradation of organic matter in a simple porous system using the 3-D diffusion-based model MOSAIC. *Biogeosciences* ; 11 :2201–2209

Qingrong Xiong, Andrey P Jivkov, John R Yates, 2014. Discrete modelling of contaminant diffusion in porous media with sorption. *Microporous and Mesoporous Materials* 2014 ;185 : 51–60

O Monga, M Bousso, P Garnier, V Pot, 2008. 3-D geometrical structures and biological activity: application to soil organic matter microbial decomposition in pore space. *Ecological Modelling* ; Vol. 216 :291–302

O. Monga, M. Bousso, V. Pot, P. Garnier Using pore space 3D geometrical modelling to simulate biological activity: impact of soil structure, 2009. *Computers and Geosciences*, 35, 2009.

Alfio Quarteroni, Riccardo Sacco, Fausto Saleri, *Méthodes Numériques – Algorithmes, analyse et applications*, 2007. Springer

be

Alain Trésor Kemgue, Olivier Monga, Serge Moto, Valérie Pot, Patricia Garnier, and Philippe C. Baveye, 2019. From spheres to ellipsoids: Speeding up considerably the morphological modeling of pore space and water retention in soils. *Computers & Geosciences* 123 (2019) 20-37.

Mbe B, Monga O. et al. Scenario modelling of carbon mineralization in 3D soil architecture at the microscale: Toward an accessibility coefficient of organic matter for bacteria. *European Journal of Soil Science*. doi 10.1111/ejss.1314, August 2021.

F. Ngom, O. Monga, M. Ould Mohamed, 2012. 3D segmentation of soil micro-structures using generalized cylinders. *Computers & Geosciences*.

Ngom N. F., Garnier P., Monga Olivier, Peth S. Extraction of three-dimensional soil pore space from microtomography images using a geometrical approach, 2011. *Geoderma*, 163 (1-2), p. 127-134. ISSN 0016-7061

O. Monga. Defining and computing stable representations of volume shapes from

discrete trace using volume primitives : application to 3D image analysis in soil science, 2007. *Image and Vision Computing* 25, 1134-1153.

Mingzhu Sun, Hui Xu, Xingjuan Zeng, Xin Zhao, 2017. Automated numerical simulation of biological pattern formation based on visual feedback simulation framework. *PLOS one*, <https://doi.org/10.1371/journal.pone.0172643>

D. Nguyen-Ngoc, B. Leye, O. Monga, P. Garnier, N. Nunan. Simulating biological dynamics using partial differential equations: application to decomposition of organic matter in 3D soil structure. *Vietnam Journal of Mathematics*, Springer Verlag, 2015.

D. Nguyen-Ngoc, B. Leye, O. Monga, P. Garnier, N. Nunan. Modeling microbial decomposition in real 3D soil structures using partial differential equations. *International Journal of geosciences*, 2013, 4, 15-26, <http://dx.doi.org/10.4236/ijg.2013.410A003>

Uduak Z. George, Angelique Stephanou, Anotida Madzvamuse, 2013. Mathematical modelling and numerical simulations of actin dynamics in the eukaryotic cell. *J Math Biol*. 2013 Feb;66(3):547-93. doi: 10.1007/s00285-012-0521-1. Epub 2012 Mar 21

Kumi Francis 2015. Review of applying X-ray computed tomography for imaging soil-root physical and biological processes *International Journal of Agricultural and Biological Engineering* 8(5):1-14 ·

Y Gutiérrez, D Ott, M Töpperwien, T Salditt, 2018. X-ray computed tomography and its potential in ecological research: A review of studies and optimization of specimen preparation, *Ecology*. Wiley Online Library

Dong, H., Blunt, M.J., 2009. Pore-network extraction from micro-computerized-tomography images. *Physical Review E* 80(3), 036307.

Adolf Fick, « Über Diffusion », *Annalen der Physik und Chemie*, vol. 94, 1855, p. 59–86

Hazlett, R.D., 1995. Simulation of capillary-dominated displacements in microtomographic images of reservoir rocks. *Transport in Porous Media* 20(1-2), 21-35.

Hilpert, M., Miller, C.T., 2001. Pore-morphology-based simulation of drainage in totally wetting porous media. *Advances in Water Resources* 24(3-4), 243-255.

Jiang, Z., Wu, K., Couples, G., van Dijke, M.I.J., Sorbie, K.S., Ma, J., 2007. Efficient extraction of networks from three-dimensional porous media. *Water Resources Research* 43(12).

Plougonven, E., Bernard, D., 2011. Optimal removal of topological artefacts in microtomographic images of porous materials. *Advances in Water Resources* 34(6), 731-736.

- Reeves, P.C., Celia, M.A., 1996. A functional relationship between capillary pressure, saturation, and interfacial area as revealed by a pore-scale network model. *Water Resources Research* 32(8), 2345-2358.
- Sheppard, A., Sok, R., Averdunk, H., 2005. Improved pore network extraction methods, *International Symposium of the Society of Core Analysts*, pp. 1-11.
- Vogel, H.-J., Roth, K., 2001. Quantitative morphology and network representation of soil pore structure. *Advances in Water Resources* 24, 233-242.
- D. Nguyen-Ngoc, B. Leye, O. Monga, P. Garnier, N. Nunan, 2015. Simulating biological dynamics using partial differential equations: application to decomposition of organic matter in 3D soil structure. *Vietnam Journal of Mathematics*, Springer Verlag.
- Ruth E. Falconer, James L. Bown, Nia A. White, John W Crawford, 2008. Modeling interactions in Fungi. *J R Soc Interface*, Jun 6, 5(23): 603-615
- A Juyal, T Eickhorst, R Falconer, PC Baveye, A Spiers, W Otten, 2018. Control of pore geometry in soil microcosms and its effect on the growth and spread of *Pseudomonas* and *Bacillus* sp. *Frontiers in Environmental Science* 6, 73
- H. Resat, V. Bailey, LA McCue, A Konopka , 2012. Modeling microbial dynamics in heterogeneous environments: growth on soil carbon sources. *Microbial ecology*, Volume 63, issue 4, pp 883-897

Schaap MG, Porter ML, Christensen BSB, Wildenschild D, 2007. Comparison of pressure-saturation characteristics derived from computed tomography and lattice Boltzmann simulations. *Water Resour Res*;43:W12506.<http://dx.doi.org/10.1029/2006WR005730>.

Shan X, Chen, 1993. H. Lattice Boltzmann model for simulating flows with multiple phases and components. *Phys Rev E* ; 47(3):1815-20.

Shan X, Chen H. Simulation of non ideal gases and liquid-gas phase transitions by the lattice Boltzmann equation, 1994. *Phys Rev E* ; 49 (4) :2941-8.

Sukop MC, Huang H, Lin CL, Deo MD, Oh K, Miller JD, 2008. Distribution of multiphase fluids in porous media : comparison between lattice Boltzmann modeling and micro-x-ray tomography. *Phys Rev E* ;77:026710.